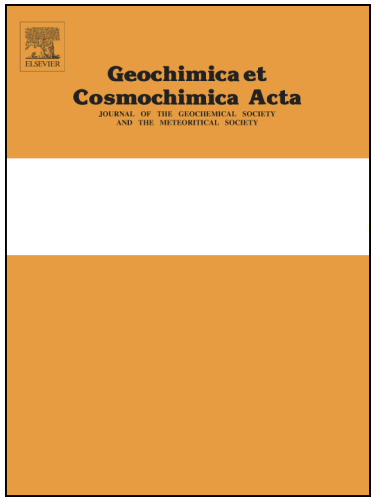

Li/Mg Systematics in Scleractinian Corals: Calibration of the Thermometer

Paolo Montagna, Malcolm McCulloch, Eric Douville, Matthias López Correa, Julie Trotter, Riccardo Rodolfo-Metalpa, Delphine Dissard, Christine Ferrier-Pagès, Norbert Frank, André Freiwald, Steve Goldstein, Claudio Mazzoli, Stephanie Reynaud, Andres Rüggeberg, Simone Russo, Marco Taviani

PII: S0016-7037(14)00093-3
DOI: http://dx.doi.org/10.1016/j.gca.2014.02.005
Reference: GCA 8661

To appear in: *Geochimica et Cosmochimica Acta*

Received Date: 16 August 2013
Accepted Date: 3 February 2014

Please cite this article as: Montagna, P., McCulloch, M., Douville, E., Correa, M.L., Trotter, J., Rodolfo-Metalpa, R., Dissard, D., Ferrier-Pagès, C., Frank, N., Freiwald, A., Goldstein, S., Mazzoli, C., Reynaud, S., Rüggeberg, A., Russo, S., Taviani, M., Li/Mg Systematics in Scleractinian Corals: Calibration of the Thermometer, *Geochimica et Cosmochimica Acta* (2014), doi: http://dx.doi.org/10.1016/j.gca.2014.02.005

Li/Mg Systematics in Scleractinian Corals: Calibration of the Thermometer

Paolo Montagna[a,b,*], Malcolm McCulloch[c,d], Eric Douville[b], Matthias López Correa[e], Julie Trotter[c], Riccardo Rodolfo-Metalpa[f], Delphine Dissard[c,d], Christine Ferrier-Pagès[g], Norbert Frank[h], André Freiwald[i], Steve Goldstein[j], Claudio Mazzoli[k], Stephanie Reynaud[g], Andres Rüggeberg[l], Simone Russo[m], Marco Taviani[a]

[a] Istituto di Scienze Marine, Consiglio Nazionale delle Ricerche, via Gobetti 101, I-40129 Bologna, Italy

[b] Laboratoire des Sciences du Climat et de l'Environnement, Av. de la Terrasse, 91198 Gif-sur-Yvette, France

[c] The UWA Oceans Institute and School of Earth and Environment, The University of Western Australia, Crawley 6009, Western Australia, Australia

[d] ARC Centre of Excellence in Coral Reef Studies, The University of Western Australia, Crawley 6009, Western Australia, Australia

[e] GeoZentrum Nordbayern, Universität Erlangen-Nürnberg, Loewenichstr. 28, D-91054 Erlangen, Germany

[f] CoRéUs, Institut de Recherche pour le Développement, Centre IRD de Noumea, 98848 Noumea, New Caledonia

[g] Centre Scientifique de Monaco, Av. Saint Martin, MC-98000 Monaco

[h] Institut für Umweltphysik, Universität Heidelberg, Im Neuenheimer Feld 229, 69120 Heidelberg, Germany

[i] Senckenberg am Meer, Abteilung für Meeresforschung, Südstrand 40, D-26384 Wilhelmshaven, Germany

[j] Lamont-Doherty Earth Observatory, Columbia University, 61 Route 9W, Palisades, NY 10964, USA

[k] Dipartimento di Geoscienze, Università degli Studi di Padova, Via G. Gradenigo 6, 35131, Padova, Italy

[l] Dept. of Earth Sciences, University of Fribourg, Chemin du Musée 6, CH-1700 Fribourg, Switzerland

[m] Institute for Environment and Sustainability, Joint research Centre, Via Enrico Fermi 2749, 21027, Ispra, Italy

* Corresponding author at: Istituto di Scienze Marine (ISMAR), Consiglio Nazionale delle Ricerche, Via Gobetti 101, 40129 Bologna (Italy), E-mail address: paolo.montagna@bo.ismar.cnr.it (P. Montagna).

ABSTRACT

We show that the Li/Mg systematics of a large suite of aragonitic coral skeletons, representing a wide range of species inhabiting disparate environments, provides a robust proxy for ambient seawater temperature. The corals encompass both zooxanthellate and azooxanthellate species (*Acropora* sp., *Porites* sp., *Cladocora caespitosa*, *Lophelia pertusa*, *Madrepora oculata* and *Flabellum impensum*) collected from shallow, intermediate, and deep-water habitats, as well as specimens cultured in tanks under temperature-controlled conditions. The Li/Mg ratios observed in corals from these diverse tropical, temperate, and deep-water environments are shown to be highly correlated with temperature, giving an exponential temperature relationship of: Li/Mg (mmol/mol) = 5.41 exp (−0.049 * T) (r^2 = 0.975, n = 49). Based on the standard error of the Li/Mg versus temperature correlation, we obtain a typical precision of ± 0.9°C for the wide range of species analysed, similar or better than that of other less robust coral temperature proxies such as Sr/Ca ratios.

The robustness and species independent character of the Li/Mg temperature proxy is shown to be the result of the normalization of Li to Mg, effectively eliminating the precipitation efficiency component such that temperature remains as the main controller of coral Li/Mg compositions. This is inferred from analysis of corresponding Li/Ca and Mg/Ca ratios with both ratios showing strong microstructure-related co-variations between the fibrous aragonite and centres of calcification, a characteristic that we attribute to varying physiological controls on growth rate. Furthermore, Li/Ca ratios show an offset between more rapidly growing zooxanthellate and azooxanthellate corals, and hence only an approximately inverse relationship to seawater temperature. Mg/Ca ratios show very strong physiological controls on growth rate but no significant dependence with temperature, except possibly for *Acropora* sp. and *Porites* sp. A

strong positive correlation is nevertheless found between Li/Ca and Mg/Ca ratios at similar temperatures, indicating that both Li and Mg are subject to control by similar growth mechanisms, specifically the mass fraction of aragonite precipitated during calcification, which is shown to be consistent with a Rayleigh-based elemental fractionation model.

The highly coherent array defined by Li/Mg versus temperature is thus largely independent of coral calcification mechanisms, with the strong temperature dependence reflecting the greater sensitivity of the $K_d^{Li/Ca}$ partition coefficient relative to $K_d^{Mg/Ca}$. Accordingly, Li/Mg ratios exhibit a highly coherent exponential correlation with temperature, thereby providing a more robust tool for reconstructing paleo-seawater temperatures.

1. INTRODUCTION

The temperature of the oceans is a critical parameter that not only controls key physical and chemical processes, such as ocean circulation and dissolution of CO_2, but also a wide range of biogeochemical processes that determine the physiological condition of marine organisms, and thus ultimately the structure of aquatic ecosystems and their food webs. A full understanding of both the drivers of temperature change in the ocean and its feedbacks on the Earth's climate system and ecosystems is however hampered by the lack of accurate, long-term observations of temperature. Instrumental records only partially cover the last ~150 years (Rayner et al., 2006) and knowledge of seawater temperature variability over decadal, centennial, and longer timescales is still limited, with reliable ocean-wide observations only commencing in the past few decades. The lack of longer-term ocean temperature records and its variability in both shallow and deep-water environments in particular, thus remain a major limitation in our understanding of the key processes controlling changes in the Earth's climate.

To overcome the lack of long-term instrumental data, the geochemical composition of carbonate skeletons from biomineralizing organisms (*e.g.* foraminifera, corals) has been widely applied as archives of seawater temperature. Isotopic (*e.g.* $\delta^{18}O$, $\delta^{88/86}Sr$, Δ_{47}) and elemental ratios (*e.g.* Sr/Ca, Mg/Ca, U/Ca, B/Ca) of the carbonate skeletons, especially of tropical and temperate aragonitic zooxanthellae-bearing corals (Beck et al., 1992; Guilderson et al., 1994; Shen and Dunbar, 1995; Mitsuguchi et al., 1996; McCulloch et al., 1999; Gagan, 2000; Montagna et al., 2007; Saenger et al., 2012), can provide useful proxy records of past ocean temperatures. However, all of these temperature proxies suffer to varying extents from other non-environmental factors (i.e. physiological processes) influencing their composition. Commonly termed "vital effects", these biological processes partly obscure the primary environmental signal and thus limit the reliability of paleoclimate reconstructions (Erez, 1978; Cohen and McConnaughey, 2003; Robinson et al., 2013). Furthermore, they can be highly variable between species and across different environmental regimes.

Azooxanthellate deep-water (or cold-water) corals are also potential archives of intermediate and bathyal water mass history (Adkins et al., 1998; Frank et al., 2004; Montagna et al., 2005, 2006; Robinson et al., 2005; Sinclair et al., 2006; McCulloch et al., 2010) but unlike shallow-water zooxanthellate corals (i.e. in symbiosis with unicellular *Symbiodinium* algae), they also have the advantage of inhabiting greater depths and a wider geographic range. Combined U-series and ^{14}C dating (Adkins et al., 1998; Mangini et al., 1998; Goldstein et al., 2001; Schröder-Ritzrau et al., 2003; McCulloch et al., 2010; López Correa et al., 2012) have demonstrated their utility for determining deep-water reservoir or ventilation ages. Their stable carbon and oxygen isotope composition has been used to reconstruct temperature variations providing a temperature controlled kinetic fractionation process of both carbon and oxygen isotopes (Smith et al., 1997,

2000). Further studies have however revealed the complex nature of such fractionation processes and the resulting limitations to derive temperature values (Adkins et al., 2003; Lutringer et al., 2005; Rollion-Bard et al., 2010). Moreover, trace element compositions have been shown to be strongly influenced by biological fractionation (Gagnon et al. 2007; Meibom et al. 2008; Montagna et al. 2005). It is thus clear that both tropical and cold-water corals, regardless of the presence (or absence) of zooxanthellae, exert a strong biological control over the internal chemical micro-environment at the site of calcification (Adkins et al., 2003; McCulloch et al., 2012). In the case of $\delta^{18}O$ for example, this results in a composition that is not in isotopic equilibrium with ambient seawater, and is thus different from that expected for inorganic aragonite precipitation (Smith et al., 2000). Accordingly, to extract reliable ocean temperatures from the geochemical signals preserved in carbonate skeletons, an improved understanding of the biochemical mechanisms controlling the precipitation of biogenic aragonite is required.

Whilst significant progress is being made in understanding the mechanisms controlling trace element incorporation into coral skeletons (*e.g*. Sinclair, 2005; Meibom et al., 2006; Mason et al., 2011), an alternative approach is to focus on proxies for which vital effects are minimal. A promising candidate is the Li/Mg temperature proxy which, in contrast to the extreme disequilibrium between $\delta^{18}O$ and $\delta^{13}C$ observed in deep-water corals (Adkins et al., 2003), shows a more coherent and systematic relationship in both deep-water as well as tropical corals (Montagna et al., 2009; Case et al., 2010; Hathorne et al., 2013, Raddatz et al., 2013). The studies by Case et al. (2010) and Raddatz et al. (2013) explored the potential of the Mg/Li temperature proxy in deep-water coral skeletons but were limited to azooxanthellate coral species from cold-water temperature regimes. Likewise, the study by Hathorne et al. (2013) has applied this proxy to tropical *Porites* corals from warm-water (24 to 28°C) environments.

Here, we examine the systematics of the Li/Mg palaeo-thermometer in aragonite skeletons of coral species that occur across a wide range of shallow, intermediate, and deep-water environments (tropical *Acropora* sp. and *Porites* sp., temperate *Cladocora caespitosa*, and the cold-water corals *Lophelia pertusa*, *Madrepora oculata* and *Flabellum impensum*), and for which *in-situ* temperatures are known from instrumental records (Tab 1). The study also includes specimens cultured in tanks under temperature-controlled conditions. We derived a single empirical calibration for Li/Mg ratios with respect to temperature ranging between 0.8 and 28°C that is generally applicable for a number of aragonitic scleractinian coral species. We show that the Li/Mg ratio provides a sensitive seawater temperature proxy that is largely independent of "vital effects", hence does not require species-specific calibrations, and which to the first order is consistent with closed system Rayleigh fractionation of Li/Mg. Furthermore, obtaining Li/Mg data is relatively simple and fast using an inductively coupled plasma quadrupole mass spectrometry (ICP-MS), with an analytical precision of about 2%, enabling temperature reconstructions to a precision of approximately ± 0.9°C

2. SAMPLES AND METHODS

2.1 SAMPLE COLLECTION

We analysed 38 living zooxanthellate (n = 11) and azooxanthellate (n = 27) coral specimens covering a wide range of environmental settings in terms of temperature (0.8 to 28°C), salinity (34.7 to 38.7), water depths (surface to 950 m), carbonate ion concentration (57 to 270 µmol/kg), and aragonite saturation levels (0.8 to 4.2) (Tab.1). These consist of the temperate coral *Cladocora caespitosa*, the tropical corals *Acropora* sp. and *Porites* sp., and the cold-water corals *Lophelia pertusa*, *Madrepora oculata*, and *Flabellum impensum* from the Mediterranean

Sea, Atlantic, Pacific and Southern Oceans. In addition, temperate (*Cladocora caespitosa*) and tropical (*Acropora* sp.) corals were also cultured in aquaria under different temperature regimes.

2.1.1 *Cladocora caespitosa*

The scleractinian zooxanthellate temperate coral *C. caespitosa* is one of the most important marine bioconstructors in the Mediterranean Sea (Laborel, 1987), thriving from a few meters to around 40 m depth (Morri et al., 1994). Three colonies of *C. caespitosa* were collected in the Gulf of La Spezia (Ligurian Sea, 44°03' N, 9°55' E) at about 7 m depth in June 2006, transported in thermostatically controlled tanks to the Scientific Centre of Monaco (CSM), and maintained in aquaria for two weeks at a similar temperature (18°C) and irradiance (60 µmol photon m^{-2} s^{-1}) as measured during sample collection. The colonies were divided into 20 nubbins (10-20 polyps each) from which calcification rates were measured, and which were subsequently prepared for geochemical analysis (~300 polyps). A total of 5 nubbins were randomly assigned to one of the four 15-litre experimental tanks and continuously supplied with flowing seawater at a rate of two litres per hour. Temperature was then gradually changed in each experimental tank at a rate of 1°C per day to reach the following treatments: 15, 18, 21 and 23°C and then maintained for another three weeks in order to acclimate the corals to these experimental conditions. Temperature was kept constant (± 0.05°C) in all tanks using heaters or a refrigerating system connected to electronic controllers. The salinity was constant at 38.5 during the experiment. At the end of the acclimation period corals were stained with a solution of 10 mg l^{-1} of Alizarin Red S (Dodge et al., 1984) for a period of 24h. The stain is incorporated into a thin layer of the skeleton and provides a marker for measuring skeletal growth. Corals were then

maintained for another 87 days and were naturally fed from the unfiltered seawater, which was not supplemented by artificial food products.

Calcification rates were measured at the end of the experiment using the alkalinity anomaly technique (Chisholm and Gattuso, 1991). The linear extension of the newly formed aragonite (defined as the skeleton precipitated above the Alizarin Red S marker) was measured on 20 corallites for each temperature treatment using a micrometer and binocular microscope.
All data were tested for assumptions of normality and homoscedasticity by the Cochran' test and were log-transformed when required. One-way ANOVAs were used to test the effect of temperature treatments (15, 18, 21, and 23°C). When ANOVAs showed significant differences, Tukey honest test (HSD) attributed differences between treatments. Statistical analyses were performed using STATISTICA® software (StatSoft, Tulsa, USA). Significant differences were assessed at $P < 0.05$.

2.1.2 *Acropora* sp. and *Porites* sp.

Acropora and *Porites* are among of the most diverse and widespread extant genera of reef-building zooxanthellate corals, with their geological origins traced back to the Oligocene (Wallace, 1999). Thirty six nubbins of *Acropora* sp. were collected from a single parent colony, adhered onto glass slides using underwater epoxy (Devcon®) and randomly distributed in 30-litre incubation tanks, following the protocol described by Reynaud-Vaganay et al. (1999). All nubbins were acclimated for 9 weeks at constant temperature (25°C) and irradiance (200 µmol photons m^{-2} s^{-1}). The nubbins were then randomly distributed in six tanks and cultivated for 15 weeks at different temperature (22, 25 and 28°C) and irradiance (200 and 400 µmol photons m^{-2} s^{-1}) conditions. At completion of the experiment, the skeletal material deposited on the glass slide

during the incubation period was removed with a scalpel and stored in glass containers for geochemical analyses. By sampling only the material covering the glass slide, this method allows easy collection of newly-formed aragonite, ensuring it was precipitated under the targeted culture conditions (see Dissard et al., 2012 for further experimental details). For the present study only the geochemical compositions of the coral samples grown at 200 µmol photons m^{-2} s^{-1} were measured.

Three specimens of *Porites* sp. were live-collected by SCUBA diving in the Equatorial Pacific (Tahiti and New Caledonia) and the Great Barrier Reef (Myrmidon Reef) (Tab. 1). The Japanese coral reference material JCp-1, a *Porites* coral skeleton collected from Ishigaki Island (Okai et al., 2002), was also analysed during this study.

2.1.3 *Lophelia pertusa, Madrepora oculata* and *Flabellum impensum*

Lophelia pertusa and *Madrepora oculata* are major frame-building cold-water coral species thriving at different water depths, from several tens of meters to 1 to 2 thousand meters (Zibrowius, 1980; Cairns and Stanley, 1982; Rogers, 1999). These azooxanthellate species are widely distributed in the ocean, although they are mostly found along the eastern Atlantic continental margin of NW Europe. To date, however, the full extent of the present geographic distribution remains unknown (Freiwald et al., 2004). *Madrepora* and *Lophelia* are documented since the Mesozoic and Neogene respectively (Stolarski and Vertino, 2012; Taviani et al., 2005; Vertino et al., 2013).

Twenty five specimens of *L. pertusa* were collected live from the Atlantic Ocean and the Mediterranean Sea from water depths between 105 m (Oslo Fjord) and 950 m (Darwin Mounds) and seawater temperatures between 5.9°C in the Stjernsund Reef (Norway) and 13.8°C in the

Mediterranean Sea (Tab. 1, Fig. 1). A living specimen of *M. oculata* was retrieved from the Galicia Bank (Spain) between 775 and 880 m water depth at 11.2°C.

Flabellum impensum is a solitary coral widely distributed in the Southern Ocean, including Antarctic waters (Cairns and Keller, 1993). It was collected live near Balleny Island (Antarctica) at 760 m depth (Tab. 1, Fig. 1).

2.2. SEAWATER PARAMETERS

The temperature and salinity values used in this study were mostly obtained from *in-situ* measurements using probes or CTD (conductivity, temperature, depth) profiles acquired close to the sampling locations and contemporaneously to the coral sampling (Tab. 1). Where *in-situ* measurements were not available the temperature and salinity values were selected from nearby hydrographic sites using the publically accessible GLODAP (Global Ocean Data Analysis Project) and CARINA (Carbon dioxide in the Atlantic Ocean) databases. Ambient ocean temperatures range from 0.8°C (Southern Ocean) to 27.4°C (Myrmidon Reef), and for salinity from 34.7 (Southern Ocean) to 38.7 (Mediterranean Sea).

The degree of carbonate ion saturation ($\Delta[CO_3^{2-}]$) was calculated following Yu and Elderfield (2007) ($\Delta[CO_3^{2-}] = [CO_3^{2-}]_{in\text{-}situ} - [CO_3^{2-}]_{sat}$, where $[CO_3^{2-}]_{sat} = [CO_3^{2-}]_{in\text{-}situ} / \Omega_{aragonite}$). The saturation state for aragonite (Ω_{ar}) and the *in-situ* carbonate ion concentration ($[CO_3^{2-}]_{in\text{-}situ}$) were derived from alkalinity and total dissolved inorganic carbon sourced from GLODAP and CARINA databases at stations nearby the coral sample sites. We used CO2SYS Matlab version 1.1 (Lewis and Wallace, 1998) for the CO_2 system calculations considering also *in-situ* temperature, salinity, pressure, phosphate, and silicate; the equilibrium constants K_1 and K_2 for carbonic acid are taken from the refit of Mehrbach et al. (1973) by Dickson and Millero (1987),

and the value for the solubility products for aragonite K_{sp} is from Mucci (1983). The temperature shows a significant correlation with both $\Delta[CO_3^{2-}]$ ($r^2 = 0.84$, n = 20, $p < 0.001$) and Ω_{ar} ($r^2 = 0.89$, n = 20, $p < 0.001$), as observed in most of the ocean basins.

2.3 SAMPLE PREPARATION FOR GEOCHEMICAL ANALYSIS

Different subsampling strategies were applied to the different coral species according to their skeletal structures. Twenty-seven coral fragments of *C. caespitosa* (n = 12; three corallites for each temperature experiment), *L. pertusa* (n = 14), *M. oculata* (n = 1) were selected for laser ablation ICP-MS. Prior to the analysis, the samples were sonicated three times with MilliQ water, dried overnight at 50°C, embedded in epoxy resin and cross-sectioned perpendicular (*C. caespitosa*) or parallel (*L. pertusa* and *M. oculata*) to the growth axis to completely expose the thecal wall. A small colony of *Porites* sp. from Myrmidon Reef was sliced along the main growth axis from which a 20x80 mm rectangle was cut, sonicated three times with MilliQ water and dried overnight at 50°C for laser ablation analysis.

Solution ICP-MS analyses were carried out on thirty-two small fragments (~20 mg) of the thecal wall of *C. caespitosa* (n = 12; three corallites for each temperature experiment), *L. pertusa* (n = 19) and *F. impensum* (n = 1), and on fragments (~20 mg) of *Porites* sp. (n = 3) and *Acropora* sp. (n = 3) (coral material deposited on the glass slide). The skeletal portions were physically cleaned using a small diamond bur and circular blade then finely crushed in an agate mortar. The powder was sonicated with 0.05N HNO_3 for 20 minutes to further remove potential contaminant phases. Samples were then rinsed several times with MilliQ water and dried overnight at 50°C. An aliquot of each sample was further cleaned using a sequence of oxidative and reductive steps, following the method of Lomitschka and Mangini (1999) (see below).

Elemental concentrations were analysed using ICP-MS (*C. caespitosa, Porites* sp.*, Acropora* sp.*, L. pertusa* and *M. oculata*).

2.4 Laser Ablation Quadrupole ICP-MS

A quadrupole ICP-MS (Varian 820 MS) coupled to a pulsed ArF excimer laser system (Lambda Physik LPX 120i) at the Research School of Earth Sciences, The Australian National University, was operated at 5Hz and 50mJ to measure elemental ratios *in-situ*. Measurements of the background (gas blank), NIST glass standard 614, and an in-house pressed coral standard (*Porites* from Davies Reef, Great Barrier Reef) were acquired for 60s before and after each sample run, following previously described methods (Sinclair et al., 1998; Montagna et al., 2007). The isotopes monitored were ^{7}Li, ^{25}Mg and ^{43}Ca. The NIST 614 standard was used for calibrating ^{7}Li whereas ^{25}Mg was standardized against the *Porites* pressed powder disc.

All raw counts were processed offline using ^{43}Ca as the internal standard. Slightly different analytical setups were used for the analysis of samples of *C. caespitosa*, *L. pertusa* and *Porites* sp. (see below). External reproducibility (1σ RSD) assessed by analysing the two standards was 4.5% for Li/Ca, 5.7% for Mg/Ca and 4.3% for Li/Mg.

2.4.1 *Cladocora caespitosa* and *Porites* sp.

Three corallites for each temperature experiment (15, 18, 21 and 23°C) were analysed using a 137 μm diameter laser spot, which was focused on the centres of calcification (COCs) or Rapid Accretion Deposits (Stolarski, 2003) and the surrounding fibrous aragonite (FA) or Thickening Deposits (Stolarski, 2003). Prior to analysis, the coral surface was pre-ablated twice using a 230 μm spot in order to remove possible surface contaminants. For each corallite a

minimum of three COCs and three FA portions were ablated for 20 s, producing a crater depth of ~10µm and an average of 40 element/Ca values per point. The elemental composition for each coral microstructure of the three corallites was subsequently averaged to obtain a mean value (±1σSD), representative of each temperature experimental setup.

The *Porites* sp. sample was analysed using a rectangular slit 50 µm wide and 400 µm long following a 4 cm transect along the growth axis, which began 3 cm below the living surface to avoid organic tissue remains.

2.4.2 *Lophelia pertusa* and *Madrepora oculata*

Two continuous parallel laser tracks (~2 mm apart) were ablated across the thecal wall of all of the *L. pertusa* and *M. oculata* specimens, from the external edge of the exoskeleton towards the centre, and perpendicular to the coral growth axis. The laser beam was masked using a rectangular slit 20 µm wide and 220 µm long, the latter parallel to the growth bands. The element/Ca ratios of the two tracks were combined to produce mean values for COCs, FA and the entire transect.

Following laser ablation analyses, the same thecal portions were subsampled for oxygen and carbon isotope analysis using a Merchantec MicroMill (New Wave Research) at 100 µm intervals. The carbonate powders (~100 µg subsamples) were analysed using a ThermoFinnigan MAT 252 mass-spectrometer at the Geology Department of the University of Erlangen-Nuremberg. All $\delta^{18}O$ values are reported in ‰ relative to VPDB.

2.4.3 Solution Quadrupole ICP-MS

The coral powders were dissolved in ultraclean nitric acid to obtain solutions of 100ppm Ca in 0.5N HNO_3. Bulk Li, Mg and Ca concentrations of deep-water and tropical corals were analysed using a quadrupole ICP-MS X-seriesII at LSCE (Gif-sur-Yvette, France) and a quadrupole ICP-MS ExCell at LDEO (New York, USA). The isotopes of ^{7}Li, ^{24}Mg, ^{25}Mg, ^{43}Ca, ^{44}Ca and ^{48}Ca, were used to determine multi-element concentrations, calibrated using a multi-element standard and 100 ppm Ca matrix solution of JCp-1 in 0.5N HNO_3. Sample solutions were introduced into the ICP-MS at 100 µL/min uptake using a PFA micro-nebulizer. Blanks (0.5N HNO_3) and carbonate standards JCp-1 (tropical coral) and JCt-1 (giant clam) (Okai et al., 2002) were routinely analysed to bracket samples, monitor ICP-MS drift over time, and for inter-laboratory comparisons between the two laboratories. The values and external reproducibility (1σ) obtained for JCp-1 were Li/Ca = 6.01 µmol/mol (±1.7%), Mg/Ca = 4.21 mmol/mol (±0.7%) and Li/Mg = 1.43 mmol/mol (±1.6%). Different cleaning procedures were tested on powders of nine cold-water and tropical corals, including JCp-1, before dissolution in order to evaluate the impact of the cleaning protocol on molar Li/Mg ratio. Such cleaning treatments, slightly modified from the work of Lomitschka and Mangini (1999), consisted of: 1) a weak acid treatment using 0.01N HNO_3; 2) a weak acid treatment using 0.05N HNO_3; 3) a weak acid step followed by an oxidative treatment of 0.05N HNO_3 + H_2O_2/NaOH at 80°C; and 4) a weak acid step, an oxidative step, and a final reductive treatment using 0.05N HNO_3 + H_2O_2/NaOH + ascorbic acid/EDTA. The geochemical analyses of JCp-1 showed comparable variations in Li/Ca and Mg/Ca ratios between the different cleaning steps (Table 2). Accordingly, Li/Mg ratio did not show any significant difference in the Li/Mg ratios between the treated and the untreated samples, with all values being within the analytical uncertainties. Solution ICP-MS values reported in table 3 correspond to untreated samples.

3. RESULTS

3.1 Coral calcification and linear extension of cultured *C. caespitosa* and *Acropora* sp.

Coral calcification of *C. caespitosa* showed a strong temperature dependence (ANOVA, $F_{3,16} = 4.34$, $p = 0.020$), with corals maintained at 15°C displaying a lower calcification rate than those at higher temperatures (Tukey, 15 <18 = 21 = 23°C, $p < 0.05$). Significant differences were also found for extension rate measured along the growth axis of the corallites over the whole incubation period. Extension rate increased linearly with temperature from 15°C to 21°C but decreased by 36% at 23°C relative to values determined at 21°C (ANOVA, $F_{3,298} = 69,36$, $p < 0.0001$; Tukey, 15 < 18 = 23 < 21°C)

Coral calcification of *Acropora* sp. increased linearly with increasing temperature and light conditions from 0.14 g cm^{-2} yr^{-1} at 200 µmol photons m^{-2} s^{-1} and 22°C to 0.4 cm^{-2} yr^{-1} at 400 µmol photons m^{-2} s^{-1} and 28°C (see Dissard et al., 2012 for further details).

3.2 Fine-scale trace element and stable isotope variations in coral skeletons

The laser ablation ICP-MS fine-scale analyses across different skeletal micro-structures of *L. pertusa*, *M. oculata*, *C. caespitosa*, and *Porites* sp. revealed significant variations in Li/Ca and Mg/Ca ratios (Table 3). These variations are strongly related to microstructure and are common in both zooxanthellate and azooxanthellate corals.

3.2.1 *Lophelia pertusa*

Figure 2a shows the distribution of Li/Ca and Mg/Ca ratios from laser ablation analyses across the thecal wall of *L. pertusa* collected from Propeller Mound (sample POS-265-499),

together with micro-scale variations in the oxygen isotope composition ($\delta^{18}O$) of micro-milled subsamples. All of the other specimens of *L. pertusa* and *M. oculata* analysed in the present study display similar elemental and isotopic patterns hence the observations reported herein are valid for all these cold-water coral samples. The elemental ratios along the entire transect show variations of a factor of 2 to 3, ranging from 6 to 16 µmol/mol for Li/Ca and 2 to 4.25 mmol/mol for Mg/Ca. The two ratios co-vary strongly and show a positive correlation along the entire laser ablation track ($r^2 = 0.58$; p-value <0.0001). In the coral portion corresponding to the FA (the first two millimetres from the external wall), Li/Ca and Mg/Ca show high-frequency micro-scale oscillations, with variabilities of about 28% and 20% (2σstandard deviation) respectively. COCs are significantly enriched in Li/Ca and Mg/Ca compared to the FA (+ 120% for Li/Ca and + 100% for Mg/Ca). These fine-scale trace element variations have an average width along the x-axis (*i.e.* radial) of about 200 µm with amplitudes larger than the analytical uncertainties, and closely match the skeletal microstructures visible on the transverse section of the corallite.

Variations in $\delta^{18}O$ obtained along the same track closely mimic the elemental pattern (Fig. 2a) with more negative and positive values corresponding to COCs and FA, respectively. However, due to the lower sampling resolution the high frequency variability is missing. In this study, the $\delta^{18}O$ profiles are used to help identify the coral portion precipitated closest to isotopic equilibrium with the ambient seawater. Further details regarding the correlation between trace elements and stable isotopes at micro-meter scale will be presented in a follow-up paper.

The Li/Ca versus Mg/Ca ratio, hence Li/Mg (Fig. 2b), displays an overall variation that ranges from 2.3 to 4.4 mmol/mol and a high-frequency oscillation of 25% (2σstandard deviation of the first 2 mm distance from the outer edge of the thecal wall, which corresponds to 185 laser ablation points). This oscillation is comparable to that of Li/Ca (28%) and Mg/Ca (17%).

However, the Li/Mg ratio shows little difference between the COCs and FA, and the general Li/Mg trend does not follow the oxygen isotope pattern. The shaded area in Figure 2 corresponds to a selected portion within the FA (hereafter called FA_{eq}), characterized by oxygen isotope values close to the expected isotopic equilibrium with ambient seawater ($\delta^{18}O_{eq}$ = 2.8 ± 0.2‰). This value was calculated from the seawater oxygen isotope composition (0.55 ± 0.09‰ $\delta^{18}O_{sw}$ VSMOW) and *in-situ* temperature (T = 9.6°C) using the equation by Grossman and Ku (1986) for temperature dependent oxygen isotope fractionation of aragonite. By using FA_{eq} we aim to minimize differences among coral portions that may be linked to different growth rates or related to temporal variations in the mass fraction of aragonite secreted by the organism (see discussion below).

3.2.2 *Cladocora caespitosa* and *Porites* sp.

Figure 3 shows the values for calcification rate and linear extension as well as the Li/Ca, Mg/Ca and Li/Mg ratios against temperature for the cultured *C. caespitosa* specimens. The element/Ca ratios plotted were obtained by laser ablation ICP-MS and represent the fibrous aragonite portion (see 2.4.1). The Li/Ca ratios are inversely correlated to the water temperature of the tanks and display an exponential regression, with values ranging from 11 to 7.36 µmol/mol. On the contrary, the values of Mg/Ca remain substantially constant within error. The resulting Li/Mg ratios decrease exponentially from 2.65 to 1.79 mmol/mol, following the temperature and independently from calcification or extension rate.

The laser ablation track of the *Porites* sp. specimen from Myrmidon Reef shows a positive correlation between Li/Ca and Mg/Ca ratios (r^2 = 0.38; Figure 4). In particular, the correlation is stronger during summer periods (r^2 = 0.71) compared to winter periods (r^2 = 0.48).

The Mg/Ca ratios exhibit a seasonal cycle with higher values during summer whereas the concentration difference of Li/Ca between summer and winter is not statistically significant. The Li/Mg ratio shows a clear seasonal cycle with high values corresponding to the winter periods and vice versa.

3.3 Dependence of coral Mg/Ca, Li/Ca, and Li/Mg ratios on temperature, salinity, and ΔCO_3^{2-}

Figure 4 shows the Mg/Ca, Li/Ca, and Li/Mg ratios of all the samples analysed by solution and laser ablation ICP-MS (FA_{eq} and COCs) plotted against ambient seawater temperature, salinity, and ΔCO_3^{2-} concentration. The Li/Ca ratios are inversely correlated with the seawater temperature for both the zooxanthellate and azooxanthellate coral samples, whereas Mg/Ca shows a weak negative correlation with temperature only for *L. pertusa*. The Mg/Ca and Li/Ca ratios for the FA_{eq} of *L. pertusa* decrease with increasing temperature, the sensitivity being ~3% and ~6% per °C respectively. The Li/Ca ratios of *C. caespitosa* decrease with increasing temperature, with a sensitivity of ~5% per °C, whereas the Mg/Ca values do not show any significant dependence on temperature. There is a significant Li/Ca and Mg/Ca offset between the shallow and deep-water corals, with different coral species growing at similar seawater temperatures (*e.g.* 14 to 15°C) displaying differences of ~55% for Mg/Ca and 35% for Li/Ca. Within the FA_{eq} of *L. pertusa*, seawater temperature accounts for ~18% and ~49% of the Mg/Ca and Li/Ca variances respectively, and for ~99% of the Li/Ca variance in *C. caespitosa*. Li/Ca and Mg/Ca are less well correlated with temperature incorporating the values for the COCs or the entire transect across the thecal wall of *L. pertusa* (Tab. 4).

Solution Li/Ca ratios on bulk samples generally mimic the results obtained using laser ablation ICP-MS, showing a similar offset between shallow and deep-water corals grown at similar temperature conditions (*e.g*. 14-15°C). Solution Mg/Ca ratios also show an offset between shallow and deep-water corals but these data are more scattered compared to those obtained using laser ablation ICP-MS. It is also noted that the Mg/Ca ratios for *Acropora* sp. and partly for *Porites* sp. increase with increasing temperature, as often reported for tropical corals (*e.g*. Mitsuguchi et al., 1996; Fallon et al., 2003).

We tested the possible influence of other environmental parameters on the element/Ca ratios, such as salinity, $\Delta[CO_3^{2-}]$, and the saturation state of aragonite (Ω_{ar}) (Fig. 5 and Tab. 4). Salinity does not play an obvious role in the incorporation of Li/Ca, Mg/Ca and Li/Mg into coral aragonite as shown by the scatter within the two major salinity ranges of 35 to 36 for the Atlantic, versus 38.5 to 38.7 for the Mediterranean samples. In fact, corals growing in similar saline conditions have significantly different element/Ca values, which show no correlation with salinity. Normalizing element/Ca ratios to a constant temperature by using the observed mean trends would even further reduce small differences between salinity ranges. Notably, this is consistent with the Li/Ca results of inorganic aragonite precipitated over a wide range of salinity, from 10 to 50‰ (Marriott et al., 2004a).

Li/Ca, Mg/Ca and Li/Mg ratios show variable degrees of correlations with $\Delta[CO_3^{2-}]$ and Ω_{ar}, depending on the data subset considered (see Tab. 4). Since both environmental parameters are highly correlated to temperature (r^2 = 0.84 and 0.89 for $\Delta[CO_3^{2-}]$ and Ω_{ar}, respectively), it is very likely that most of the correlation with element/Ca ratios is controlled by the temperature-induced variations of $\Delta[CO_3^{2-}]$ and Ω_{ar}. Furthermore, the correlations are eliminated when

considering the Li/Ca, Mg/Ca, and Li/Mg ratios against the ΔCO_3^{2-} and Ω_{ar} residuals (i.e. measured Ω_{ar} - Ω_{ar}(T), with Ω_{ar}(T) estimated from the temperature dependence of Ω_{ar}).

4. DISCUSSION

4.1 Fine-scale variation of element contents in coral skeleton and the role of kinetic effects

The data presented here clearly show that coral physiology affects the chemical composition of the coral skeleton during biomineralization over a range of spatial scales. The high spatial resolution of geochemical measurements using laser ablation ICP-MS shows a strong relationship between trace element abundances and skeletal architecture. In highly dynamic environments of strong bottom and tidal currents within the thermocline, such as on the slopes off Ireland and in canyons of the Mediterranean Sea, framework-forming cold-water corals are exposed to diurnal, seasonal, and annual temperature variations on the order of 1-3°C (Rüggeberg et al., 2007; Mienis et al., 2007). Assuming a temperature dependence of element/Ca incorporation as given by Figure 5, the large variations in Li/Ca and Mg/Ca ratios over short distances across the thecal wall of *L. pertusa* cannot be explained by bottom water temperature fluctuations. If the fine-scale variations in Mg/Ca (Fig. 2) are converted to seawater temperature using the equation by Mitsuguchi et al. (1996), the calculated range would be equivalent to ~18°C, which far exceeds the variation recorded at the sample location (~0.5°C). This implies that factors other than temperature are actively controlling the chemical composition of the different portions of the skeleton, as previously suggested for tropical and deep-water corals (*e.g.* Sinclair, 2005; Meibom et al., 2006).

The large Mg/Ca variations (factor of 2) observed in this study agree well with those reported by Cohen et al. (2006), Sinclair et al. (2006) and López Correa et al. (2010) for three

live-caught specimens of *L. pertusa* from Tisler Reef, Sula Ridge, and Santa Maria di Leuca, respectively. Comparable microstructurally-related Mg/Ca variations were also documented in the deep-water corals *Desmophyllum dianthus* (Montagna et al., 2005; Gagnon et al., 2007), *Flabellum* spp., and *Caryophyllia* spp. (Shirai et al., 2005), and in tropical corals (Meibom et al., 2006; Allison and Finch, 2007) thereby implying some common physiological mechanisms controlling the uptake of Mg in coral skeletons. Similarly, large variations in Li/Ca ratios have been previously documented within the coral skeleton of *L. pertusa* (Montagna et al., 2009; Rollion-Bard et al., 2009), *D. dianthus,* and *Balanophyllia* sp. (Case et al., 2010).

This microstructurally-related pattern of Mg/Ca and Li/Ca ratios in corals is consistent with a significant difference in growth rate between COCs and fibrous aragonite, with the latter being slower and closer to thermodynamic equilibrium. The growth rate difference (*i.e*. factor of ~4.5) between the two coral microstructures has been documented in a recent study (Brahmi et al., 2012) using ^{86}Sr-labeling and NanoSIMS imaging. In addition, our trace element and isotopic data suggest growth rate variations within the slow-growing fibrous aragonite, consistent with the existence of a highly dynamic biomineralization front (Brahmi et al., 2012).

The influence of growth rate during the incorporation of Mg/Ca and Li/Ca is not exclusive to biogenic carbonates but has also been documented for inorganic aragonite during precipitation experiments (Gabitov et al., 2008; Holcomb et al., 2009). In particular, the partition coefficients for Li/Ca and Mg/Ca ($K_d^{Me/Ca}$ = $(Me/Ca)_{solid}$ / $(Me/Ca)_{fluid}$, where Me is Li or Mg) positively correlate with precipitation rate in inorganically-precipitated aragonitic spherulites. Furthermore, Li/Ca and Mg/Ca ratios are enriched in spherulite centres relative to fibres by factors of 2 and 8, respectively (Gabitov et al., 2011). This suggests that the incorporation of Li/Ca and Mg/Ca is strongly influenced by crystal-growth kinetics, both in biogenic and abiotic

aragonite. It is important to note that the Li/Ca growth rate dependence in inorganic aragonite is weaker than that of Mg/Ca (Gabitov et al., 2011).

The enrichment of Mg/Ca ratios in the COCs of *D. dianthus* and in the inorganic aragonite spherulite centres has been explained using the surface entrapment model of Watson (2004), assuming rapid precipitation in these specific microstructures compared to fibrous aragonite (Gagnon et al., 2007; Gabitov et al., 2008, 2011; Holcomb et al., 2009). Specifically, the concentration of an element near the surface combined with the competition between crystal growth and ion migration, control the trace element and isotope composition of the newly formed crystal (Watson, 2004).

By combining our geochemical data with the Mg data from inorganic precipitates given by Gabitov et al. (2008), we can hypothesise that the portions of the thecal wall of *L. pertusa* characterized by low Mg/Ca, low Li/Ca, and high $\delta^{18}O$ values (FA_{eq}, Fig. 2) likely grew at very low growth rates close to thermodynamic equilibrium, with near 0% of surface entrapment. This is consistent with the concept described by Juillet-Leclerc et al. (2009) for tropical and deep-water corals, in which the aragonite fibres experience the full range of kinetic conditions between thermodynamic equilibrium to disequilibrium. These specific coral portions can potentially retain unbiased environmental signals and so are the most suitable components to target for micro-scale geochemical analyses (*e.g.* laser ablation ICP-MS, ion microprobe, and micromilling). Indeed, correlations between Li/Ca, Mg/Ca and Li/Mg ratios with temperature significantly improve when considering only these micro-portions (Tab. 4).

The correlation between Mg/Ca and coral growth rate is also evident at the macroscopic scale (Swart, 1981; Inoue et al., 2007; Reynaud et al., 2007). In particular, Reynaud et al. (2007) found a significant correlation between Mg/Ca and the calcification rates of several nubbins of

Acropora sp. cultured at five different temperatures, concluding that the rate of calcification may exert a strong control on the Mg/Ca ratio in the coral skeleton. These results were recently used by Gaetani et al. (2011) to demonstrate the precision and accuracy of their approach for extracting temperature information, based on Rayleigh fractionation and the combined use of multiple elemental ratios.

4.2 Mechanisms of incorporation for Li and Mg in coral skeletons

Unlike Sr^{2+} or Ba^{2+}, Mg^{2+} does not substitute directly for Ca^{2+} in aragonite due to the smaller ionic radius of Mg^{2+} (0.89 Å for Mg^{2+} compared to 1.12 Å for Ca^{2+} for coordination number 8; Shannon, 1972). This is expected given that ionic substitution does not commonly occur in aragonite when the ionic radius of an element differs by more than 15% from that of calcium (Goldschmidt, 1954). Since Mg^{2+} is too small to stably occupy the Ca^{2+} site in the aragonite lattice and the difference of radii would create a lattice strain, it is more likely that Mg^{2+} is adsorbed on crystal discontinuities or incorporated into lattice defects, as suggested for example by Mitsuguchi and Kawakami (2012) for potassium and sodium. Another possibility is that Mg is hosted by a disordered Mg-bearing material, such as organic material or amorphous calcium carbonate (ACC) (Finch and Allison, 2008). However, as also discussed in Meibom et al. (2004), if Mg were associated with an organic phase, variations in the Mg and Ca concentrations would be correlated. This is not the case in our study since the laser ablation ICP-MS results of *L. pertusa* and *Porites* sp. show that higher concentration of Mg does not correspond to lower Ca values and the two elements are not correlated. The presence of ACC as a precursor to the formation of the COCs in corals was also suggested by Rollion-Bard et al.

(2010), based on the lack of a suitable mechanism that explains low Sr/Ca and oxygen, carbon, and boron isotopic values, together with increased Mg/Ca in the COCs relative to the FA.

Similarly, the substitution of Li^+ for Ca^{2+} is also unlikely to occur stoichiometrically. Moreover, non-isovalent metal partitioning is complicated by the need for charge balance to maintain neutrality in the crystal structure, either by the development of intrinsic vacancies or a coupled substitution by a second trace element. However, at present the lack of inorganic aragonite precipitation experiments at different temperatures represents a major limitation in our understanding of the mechanisms of Li incorporation into aragonite. Based on the positive correlation between Mg/Ca and Li/Ca ($r^2 = 0.58$; p-value < 0.0001) (Fig. 2), and the fact that both elements have very small partition coefficients as well as similar ionic radii (0.92 Å for Li^+ for coordination number 8; Shannon, 1972), it is most likely that the uptake mechanism is similar for both elements, and comparable biological and physicochemical factors are regulating their distribution within the coral skeleton (Case et al., 2010; Hathorne et al., 2013; Raddatz et al., 2013). However, contrary to Hathorne et al. (2013), our results from *Porites* show a positive correlation between Li/Ca and Mg/Ca ratios ($r^2 = 0.38$; Figure 4). Higher Mg/Ca ratios during summer compared to values in winter are consistent with results obtained from other studies on tropical corals (e.g. Mitsuguchi et al., 1996; Fallon et al., 2003). Both Mg/Ca and Li/Ca ratios at micro-meter resolution seem strongly influenced by the calcification rates, which is higher in summer than in winter. The temperature component for Li/Ca (*i.e*. negative Li/Ca vs. T correlation) is cancelled out by the effect of the precipitation rate, which controls the variation of the elemental ratio at fine-scale resolution, and undermines the use of Li/Ca as a reliable temperature proxy in *Porites*. On the other hand, the Li/Mg ratio shows a clear seasonal cycle with high values corresponding to the winter periods and vice versa. Discrepancy between our

results and those of Hathorne et al. (2013) may be related to the sampling strategies (i.e. laser ablation *vs.* drill), which imply the averaging of different material volumes for each analytical spot.

We hypothesize that both elements enter the interface between the calicoblastic cells and the underlying coral skeleton, into the extracellular calcifying medium (ECM) (Tambutté et al., 2011), following similar pathways of transport. The ECM ranges from a few nanometres (Tambutté et al., 2007) to more than 1 μm in width (Johnston, 1980; Isa, 1986; Le Tissier, 1990) and is the site where calcification occurs.

The chemical similarity between Li and Mg in solution (*e.g.* both are known to be strongly hydrated ions) likely leads to a common pathway, independently whether they enter the ECM via paracellular diffusion of seawater or transcellular transport. Based on recent coral culture experiments using enriched stable isotopes (^{43}Ca, ^{87}Sr, and ^{136}Ba) and the rare earth element Tb^{3+} (Gagnon et al., 2012), and the fact that it is unlikely that Mg and Li are transported via Ca^{2+} transport mechanisms due to their small ionic radii, we suggest a common pathway for both elements via direct seawater transport.

If direct seawater transport to the ECM occurs, then the Mg and Li concentrations in the ECM solution should be very similar to ambient seawater since extensive elemental removal (*e.g.* via Rayleigh distillation) seems unlikely during calcification, given their very small partition coefficients. However, this would not be the case for Li/Ca and Mg/Ca ratios, which would increase as the fraction of Ca remaining in the reservoir decreases during aragonite precipitation.

It is well known that corals have the ability to increase the carbonate saturation state within the ECM by manipulating the pH at the site of calcification through a plasma membrane

Ca^{2+}-ATPase present in the calicoblastic epithelium (Zoccola et al., 2004; McCulloch et al., 2012; Venn et al., 2013). Moreover, the morphological comparison between the coral microstructures and inorganically-precipitated aragonite suggests that COCs are formed at a higher saturation state compared to fibrous aragonite (Holcomb et al., 2009). The fine-scale bands observed within the coral skeleton can be explained by cycles in saturation state in the calcifying environment (Holcomb et al., 2009). This supports the bio-inorganic model proposed by Tambutté et al. (2011), in which crystal growth occurs through a primary inorganic process via manipulation of the saturation state by the coral.

Following the above rationale, we speculate that the concentrations of Mg and Li in the ECM are comparable to those of external seawater, and that the fine-scale variation of both elements in the coral skeleton is controlled primarily by the aragonite precipitation rate. This, in turn, is controlled by the saturation state that is manipulated by the coral at crystal lattice-scale, likely by secreting organic molecules or templates. Furthermore, organic molecules may play an important role in the incorporation of Mg and Li by affecting the desolvation process (i.e. the removal of the water of hydration around the ion) before the incorporation within the skeleton or by hosting high concentration of these two elements.

Although the exact mechanisms by which Mg and Li enter the ECM and are incorporated into coral aragonite remain speculative and require further investigation, we can certainly conclude that both elements are controlled by similar calcification mechanisms, and that their spatial distribution is very similar in both biogenic and abiotic aragonite (Gabitov et al., 2011).

4.3 Calibration of the Li/Mg thermometer

All of the Li/Ca ratios from solution and laser ablation ICP-MS were normalized to Mg/Ca and plotted as Li/Mg against seawater temperature (Fig. 6). For the laser ablation data, only the Li/Mg values specific to FA_{eq} were considered. The Li/Mg ratios show a much stronger correlation to temperature ($r^2 = 0.975$) compared to either Li/Ca or Mg/Ca ratios (Tab. 4), thus accounting for more than 97% of the variance. The correlation between Li/Mg and temperature for all the data considered together (i.e. shallow and deep-water corals) follows an exponential regression:

$$\text{Li/Mg (mmol/mol)} = 5.41 \exp((-0.049 \pm 0.002)*T) \quad \ldots\ldots\ldots\ldots\ldots\ldots\ldots\ldots \text{(1)}$$

($r^2 = 0.975$, $n = 49$, $p < 0.0001$)

The coefficients for the exponential relationship [Li/Mg = B*exp(A*temperature)] were calculated using a weighted linear regression between seawater temperature and the natural logarithm of Li/Mg values. The uncertainties of the coefficients were calculated considering the analytical uncertainties of the Li/Mg ratios and are reported as 2σSE, with the error of ln(B) = 0.02.

A similar intercept (5.22) and slope (-0.047) with slightly higher errors (±0.03 and ±0.003, respectively) were obtained using a bootstrap method with 1000 re-samplings. The exponential fit indicates a decrease in Li/Mg of ~5% per °C. The precision is ±0.9°C, as quantified by the standard error of estimates calculated from equation 1 (Bevington and Robinson, 1992; Runyon et al., 1996), which is similar to or better than the precision obtained using other temperature proxies in deep-water corals (*e.g.* Δ_{47}, Thiagarajan et al., 2011). The same temperature precision (±0.9°C) is obtained based on the mean difference of the Li/Mg values

(0.11 mmol/mol) from the exponential regression line. Using recently published Li/Mg data for corals from the family Caryophylliidae (Case et al., 2010), we also find that the resultant exponential regression is identical within error to equation 1. The calculated exponential equation is also identical (within error and considering the standardization procedure specific for each laboratory) to that determined for *Porites* (see Figure 6 in Hathorne et al., 2013).

4.4 The role of Rayleigh fractionation

Rayleigh fractionation is a well-known process that occurs naturally, for example, in fractional crystallization of magma, or the precipitation of rain from clouds. The Rayleigh process has been also applied to model the precipitation of trace elements in foraminiferal calcite and coral aragonite (Elderfield, 1996; Cohen et al., 2006; Gaetani and Cohen, 2006; Gagnon et al., 2007; Case et al., 2010) with the trace element composition of the precipitated calcite/aragonite changing as a function of the fraction of the Ca remaining in the biomineralization reservoir, following the Rayleigh equation (*e.g.* Albarède, 1995):

$$(Me/Ca)_{cf} = (Me/Ca)_{sw} f_{Ca}^{(K_d^{Me/Ca}-1)} \quad \ldots\ldots\ldots\ldots\ldots\ldots\ldots\ldots\ldots\ldots\ldots\ldots\ldots\ldots\ldots\ldots\ldots\ldots \quad (2)$$

where Me/Ca_{sw} and Me/Ca_{cf} are the ratios of a trace element (*e.g.* Me/Ca = Mg/Ca or Li/Ca) in seawater and the evolving calcifying fluid, and f_{Ca} is the fraction of Ca remaining in the parent solution. Following standard convention, $K_d^{Me/Ca}$ is the partition coefficient between the aragonite and the calcifying fluid and is given by:

$$K_d^{Me/Ca} = (Me/Ca)_{arag} / (Me/Ca)_{cf} \quad \ldots\ldots\ldots\ldots\ldots\ldots\ldots\ldots\ldots\ldots\ldots\ldots\ldots\ldots\ldots\ldots\ldots\ldots \quad (3)$$

and hence equation 2 becomes: $(Me/Ca)_{arag} = K_d^{Me/Ca} (Me/Ca)_{cf} f_{Ca}^{(K_d^{Me/Ca}-1)}$ …….. (4)

where Me/Ca_{arag} is the ratio of the aragonite precipitated in equilibrium with the calcifying fluid. Following the same approach as in Gagnon et al. (2007) for Sr/Ca and Mg/Ca, we calculated the log-log relationship between Li/Ca and Mg/Ca by eliminating f_{Ca} from equation 4, as both elemental ratios are controlled to the same extent by the fraction of aragonite precipitated and hence:

$$\ln(Li/Ca)_{coral} = \ln(K_d^{Li/Ca}) + \ln(Li/Ca)_{sw} + [(K_d^{Li/Ca} - 1)/(K_d^{Mg/Ca} - 1)] * [\ln(Mg/Ca)_{coral} - \ln(K_d^{Mg/Ca}) - \ln(Mg/Ca)_{sw}] \quad \ldots\ldots\ldots (5)$$

To model the measured Mg/Ca versus Li/Ca variability, we first assume that the ECM is a closed or semi-closed space where calcification occurs, and that the initial $(Mg/Ca)_{cf}$ and $(Li/Ca)_{cf}$ concentrations in the ECM are similar to those of seawater: Mg/Ca = 5.13 mol/mol (Broecker and Peng, 1982) and Li/Ca = 25.9 μmol/kg (Stoffynegli and Mackenzie, 1984).

With this condition and assuming that the partition coefficients remain constant during aragonite precipitation, the concentrations of Mg/Ca and Li/Ca in the ECM will increase as a function of f_{Ca} (Eq. 2) as more aragonite precipitates, since both elements are preferentially excluded from the aragonite structure. The coral aragonite precipitated from this fluid will evolve according to the changing composition of the fluid and, therefore, a Rayleigh model would predict a positive correlation between Mg/Ca and Li/Ca ratios.

In calculating this relationship, we first consider the Mg partition coefficient ($K_d^{Mg/Ca}$) versus temperature relationship for inorganic aragonite precipitated from seawater at different temperature conditions (Gaetani and Cohen, 2006). The $K_d^{Mg/Ca}$ shows significant negative temperature dependence (Fig. 4 in Gaetani and Cohen, 2006), with ~2% decrease per °C increase:

$$K_d^{Mg/Ca} = 0.0022 \exp(-0.0205 * T) \quad \ldots\ldots\ldots (6)$$

($r^2 = 0.99$, n = 7, $p < 0.0001$)

A negative relationship between Mg/Ca ratios and temperature was also observed by Gabitov et al. (2008) for inorganic aragonite during their precipitation experiments. However, the absolute values for $K_d^{Mg/Ca}$ obtained by Gabitov et al. (2008) are significantly lower (~$2.3x10^{-5}$ at 22°C compared to $1.33x10^{-3}$ at 25°C), likely due to the different precipitation rates used during the experiments. The $K_d^{Mg/Ca}$ values of Gaetani and Cohen (2006) are also higher than those estimated by Zhong and Mucci (1989) for inorganic aragonite (~$7x10^{-4}$), Lorens and Bender (1980) for biogenic aragonite from the bivalve *Mytilus edulis* (~$3.5x10^{-4}$), and Gagnon et al. (2007) for the cold-water coral *Desmophyllum dianthus* ($2.75x10^{-4}$). Moreover, the partition coefficients for Mg/Ca calculated from our geochemical results (Tab. 3) range between $5x10^{-4}$ and $8x10^{-4}$. Accordingly, we have modified the coefficient of equation 6 to maintain $K_d^{Mg/Ca}$ values within the observed range, thus our new equation is:

$$K_d^{Mg/Ca} = 0.00053 \exp(-0.0205 * T) \quad \text{.....(7)}$$

Based on the measured Mg/Ca and Li/Ca ratios for each coral sample (Tab. 3), the temperature-dependent $K_d^{Mg/Ca}$ (Eq. 7), Mg/Ca_{sw} and Li/Ca_{sw}, we calculated the corresponding $K_d^{Li/Ca}$ values (Table 5). These values range between $8.80x10^{-4}$ and $5.55x10^{-3}$, which are comparable to values reported by Livingston and Thompson (1971) for other scleractinian corals, Marriott et al. (2004b), and Hathorne et al. (2013) for *Porites*, Rollion-Bard et al. (2009) and Case et al. (2010) for cold-water corals, and Marriott et al. (2004a) for inorganic aragonite. The $K_d^{Li/Ca}$ values are highly correlated with ambient temperature, showing ~7% decrease per °C increase:

$$K_d^{Li/Ca} = 0.0056 \exp(-0.0675 * T) \quad \text{.....(8)}$$

($r^2 = 0.99$, n = 49, $p < 0.0001$)

The calculated exponential relationship represents the evolution of the partition coefficient of Li/Ca in aragonite and can be compared to the sensitivity of $K_d^{Li/Ca}$ to temperature for inorganically precipitated calcite (Marriott et al., 2004b). From our model it seems that the temperature-dependency of Li/Ca is slightly greater in aragonite than in calcite (6.7% compared to 4.6% in calcite).

Using the temperature-dependent $K_d^{Mg/Ca}$ and $K_d^{Li/Ca}$ values (Table 5), we then calculated the evolution of Mg/Ca and Li/Ca ratios in the aragonite, based on equation 5 for f_{Ca} ranging between 1 and 0 (Fig. 7). Figure 7 shows the results of the Rayleigh fractionation model together with the laser ablation Mg/Ca and Li/Ca ratios measured at high spatial resolution along the skeleton of some specimens of *L. pertusa*, *C. caespitosa,* and *Porites* sp.; note that only values of the fibrous portions are plotted for *L. pertusa* and *C. caespitosa*. The positive slopes of Mg/Ca versus Li/Ca are fully consistent with a Rayleigh fractionation model, with the value of each slope $[(K_d^{Li/Ca} - 1)/(K_d^{Mg/Ca} - 1)]$ being controlled by the temperature variations. Case et al. (2010) reported a match between measured Mg/Ca and Li/Ca and Rayleigh model data, however their results are limited to a single coral species (*D. dianthus*) at one temperature setting (3.2°C). Our results clearly show that the Rayleigh fractionation model explains most of the fine-scale Mg/Ca versus Li/Ca variations observed in tropical, temperate, and cold-water corals.

On dividing the calculated $K_d^{Li/Ca}$ values with the $K_d^{Mg/Ca}$ (i.e. $K_d^{Li/Mg}$) for each sample, and correlating them with temperature we obtained equation 9 (below):

$$K_d^{Li/Mg} = 10.65 \exp(-0.047 * T) \quad \text{.....(9)}$$

($r^2 = 0.98$, n = 49, $p < 0.0001$)

The exponential fit indicates a decrease in $K_d^{Li/Mg}$ of ~5% per °C, which is identical within error to the temperature sensitivity of Li/Mg obtained for the corals. The Li/Mg ratio in corals is thus controlled by the greater temperature sensitivity of $K_d^{Li/Ca}$ relative to $K_d^{Mg/Ca}$.

The Li/Ca and Mg/Ca ratios in coral are mainly driven by the effect of temperature on their partition coefficients and the effect of the precipitation efficiency (driven by changes in saturation state), which act in opposing directions. Both ratios behave very similarly with respect to Rayleigh fractionation, which results in an essentially constant Li/Mg ratio in the ECM. Consequently, temperature is ultimately the primary controller of the Li/Mg composition of coral aragonite skeletons.

5. CONCLUSIONS

This study clearly demonstrates that the Li/Mg composition of zooxanthellate and azooxanthellate coral aragonite skeletons is a relatively robust and reliable seawater temperature proxy. This has been validated using live-caught specimens occurring across a wide range of temperature regimes, as well as corals cultured in tanks under temperature-controlled conditions. The Li/Mg ratio is not influenced by variations in salinity, ΔCO_3^{2-}, or aragonite saturation state. It significantly correlates to temperature following a single exponential regression: Li/Mg (mmol/mol) = 5.41 exp (−0.049 * T) ($r^2 = 0.975$, n = 49).

Unlike Li/Mg, the Li/Ca and Mg/Ca ratios show large variations at micro-scale across the thecal wall of the cold-water coral *L. pertusa*, which are strongly related to the skeletal microstructures. Both ratios are significantly enriched in the centres of calcification compared to the fibrous aragonite, consistent with results from inorganic precipitation experiments, in which

Li/Ca and Mg/Ca ratios show higher concentrations in fast-growing spherulite centres relative to slow-growing fibres. This suggests that incorporation of Li/Ca and Mg/Ca is strongly influenced by crystal-growth kinetics, a phenomenon that is likely to operate both in biogenic and abiotic aragonite.

Comparison of our laser ablation ICP-MS data with published results from inorganic experiments suggest that the portions of the thecal wall of *L. pertusa* characterized by low Li/Ca and Mg/Ca likely grew at very low growth rate close to thermodynamic equilibrium. These fibrous portions can potentially retain unbiased environmental signals and are the best areas to target for micro-scale geochemical analyses. The distribution of Li and Mg within the coral skeleton is thus regulated by the same biological and physicochemical factors and both elements are incorporated into aragonite following similar calcification mechanisms.

We show that the fine-scale Li/Ca versus Mg/Ca variations observed in tropical, temperate, and deep-water corals closely follow a Rayleigh fractionation model, with the positive slopes of Li/Ca versus Mg/Ca being controlled by the different temperature sensitivities. When indexing Li to Mg, the resultant Li/Mg ratio reduces the effect of biological processes such that temperature is the primary controller of coral Li/Mg compositions. Li/Mg ratios can thus be used to obtain more accurate records of both surface and bathyal paleoseawater temperatures using precisely dated shallow and deep-water coral skeletons, and is generally superior to existing element/Ca temperature proxies.

ACKNOWLEDGEMENTS

This work was supported by the MISTRALS/PALEOMEX/COFIMED project, funded by the French CNRS and CEA, by the national project INSU/LEFE/PHARE and the European Project

on Ocean Acidification (EPOCA grant agreement number 211384). This work contributes to the projects HERMES (GOCE-CT-2005-511234) and HERMIONE (contract number 226354) within the 6th and 7th Framework Program of the European Commission as well as to the RITMARE project.

P Montagna is grateful for financial support from the Marie Curie International Outgoing Fellowship (MEDAT-ARCHIVES). M McCulloch, J Trotter, and D Dissard gratefully acknowledge the support provided by ARC grant DP0986505. M McCulloch and D Dissard were also supported by the ARC Centre of Excellence in Coral Reef Studies. M McCulloch was a recipient of a Western Australian Premiers Fellowship kindly provided by the Western Australian Premiers Department. G Mortimer and L Kinsley provided support for the trace element and LA-ICPMS analyses conducted at ANU. A Rüggeberg acknowledges funding by Deutsche Forschungsgemeinschaft (DFG), Project TRISTAN (Du 129/37). Thanks are also extended to the captains, crews, chief scientists, and scientific parties of research cruises with RV MARION DUFRESNE (MD 01), RV METEOR (M 61/3, 70/1), RV POSEIDON (POS-228, 265, 292, 325), RV VIKTOR HENSEN (VH-95, -97), RV ALKOR (AL-232, 316) and RV Urania (COR-2).

This is LSCE contribution XXXX. This is ISMAR-CNR Bologna scientific contribution n. xxxx.

FIGURE CAPTIONS

Figure 1. Map with the locations of the coral samples analysed. 1 – Stjernsund (POS-325-433-1; POS-325-433-2; JR-111), 2 – Sula Ridge (POS-228-216; POS-228-217; VH-95-163), 3 – Oslo Fjord (ALK-232-1050 BG), 4 – Darwin Mounds (DW1383#1), 5 – NW Rockall Bank, (POS-292-525; POS-292-526-1), 6 – SE Rockall Bank (MD01-2454G; POS-292-544-1), 7 – Porcupine

Seabight (MD01-2463G; M61/3-634; POS-265-499), 8 – Galicia Bank (VH-97-351; VH-97-315), 9 – Gulf of Mexico (GoM), 10 – N'Zeta off Angola (N'Zeta), 11 – Urania Bank (M70/1-677), 12 – Apulian Bank (M70/1-721-red; M70/1-721-white; COR2-111; COR2-111(bis); COR2-84), 13 – Bari Canyon (M70/1-Dive111), 14 – Balleny Island (Fbal), 15 – Myrmidon Reef, 16 – New Caledonia (NC_2001-2004), 17 – Tahiti, Moorea (CS MOOO3A-102).

Figure 2a. Li/Ca (grey line) and Mg/Ca (black line) ratios from laser ablation ICP-MS along the thecal wall of a specimen of *Lophelia pertusa* collected in Propeller Mound (sample POS-265-499), together with micro-scale variations in the oxygen isotope composition (grey dots) of micro-milled subsamples. **b**. Li/Mg ratios along the same transect. Grey bar represents the portion of fibrous aragonite precipitated closest to the expected isotopic equilibrium with ambient seawater (FA_{eq}). COCs: centres of calcification. Horizontal thick and dotted lines represent expected isotopic equilibrium with ambient seawater ($\delta^{18}O_{eq}$ = 2.8 ±0.2‰).

Figure 3. Variations in Li/Ca, Mg/Ca and LiMg ratios compared to the calcification and linear extension rate of the coral skeleton of *Cladocora caespitosa*, cultured in experimental tanks at four different temperature conditions (15, 18, 21 and 23°C). Linear extension rate increases as temperature increases from 15°C to 21°C but decreased by 36% at 23°C compared to 21°C. Calcification is variable among the temperature treatments, with corals maintained at 15°C and 21°C displaying lower and higher calcification rate, respectively. The Li/Ca ratios are inversely correlated to the water temperature of the tanks and display an exponential regression, whereas the values of Mg/Ca remain substantially constant within error. The resulting Li/Mg ratios decrease exponentially from 2.65 to 1.79 mmol/mol, and follow temperature.

Figure 4. Li/Ca, Mg/Ca and Li/Mg ratios obtained by laser ablation ICP-MS following a 4 cm transect along the growth axis of a *Porites* sp. specimen live-collected from Myrmidon Reef. Li/Ca and Mg/Ca ratios show a positive correlation, which is stronger during the summer periods compared to the winter periods. The Mg/Ca ratios exhibit a seasonal cycle with higher values during summer in accordance to results obtained from other studies on tropical corals (e.g. Mitsuguchi et al., 1996; Fallon et al., 2003). The resulting Li/Mg shows a clear seasonal cycle with lower values corresponding to the summer and vice versa.

Figure 5. Li/Ca, Mg/Ca and Li/Mg variations for cold-water, temperate and tropical corals related to changes in temperature, salinity and ΔCO_3^{2-}. Grey and white circles represent laser ablation ICP-QMS values for fibrous aragonite and COCs, respectively. Note that for specimens of *L. pertusa* and *M. oculata* only values for FA_{eq} are plotted. Black squares represent solution ICP-MS data.

Figure 6. Laser ablation and solution ICP-QMS Li/Mg ratios versus temperature for all specimens of cold-water, temperate and tropical corals investigated in the present study. For the laser ablation data, only the Li/Mg values specific to FA_{eq} were considered. Data from Case et al. (2010) are also reported (grey circles). The Li/Mg ratios show a strong correlation to temperature ($r^2 = 0.975$) following an exponential regression with Li/Mg decreasing by ~5% per °C.

Figure 7. Laser ablation ICP-MS Li/Ca and Mg/Ca values for specimens of *L. pertusa*, *C. caespitosa* and *Porites* sp. plotted together with calculated Rayleigh model lines. Values for *L.*

pertusa and *C. caespitosa* represent fibrous aragonite. F is the fraction of Ca remaining in the parent solution. Our results show that the Rayleigh fractionation model can explain most of the fine-scale Mg/Ca versus Li/Ca variations observed in tropical, temperate and cold-water corals. However, the scatter of Li/Ca and Mg/Ca (and thus Li/Mg) for small local temperature variations points towards an additional influence on Li/Mg ratios, which must be independent of the fraction of aragonite secreted by the organism. As mentioned above, the partition coefficients for Li/Ca and Mg/Ca positively correlate with growth rate in corals and inorganically-precipitated aragonite, suggesting that both ratios are influenced to some degree by crystal growth kinetics. However, the K_d's for Li and Mg have different rate dependence, with the dependence of Mg/Ca being higher than that of Li/Ca (Gabitov et al., 2011). Therefore, the effect of this difference within the fibrous aragonite is not cancelled out when normalizing Li on Mg (Fig. 2b and 6) and a residual signal remains on the Li/Mg ratio that needs to be further investigated. Note that the difference in Li/Ca and Mg/Ca ratios between the fast-growing COCs and the surrounding fibrous aragonite due to crystal growth kinetics could overestimate the temperature reconstruction (*i.e.* lower Li/Mg). Therefore, the Li/Mg temperature proxy might not work in the presence of high amount of COCs (e.g. along the septa of some coral species) or where large differences in growth rate occur.

Table 1. Geographic coordinates and depths of the coral specimens analysed in this study with hydrographic data and carbonate system parameters. CO_3^{2-} and $\Omega_{aragonite}$ were calculated by CO2SYS Matlab version 1.1 from alkalinity and total dissolved inorganic carbon sourced from GLODAP and CARINA databases at stations nearby the coral sample sites.

$\Delta[CO_3^{2-}] = [CO_3^{2-}]_{in\text{-}situ} - [CO_3^{2-}]_{sat}$, where $[CO_3^{2-}]_{sat} = [CO_3^{2-}]_{in\text{-}situ} / \Omega_{aragonite}$).

Table 2. Li/Ca, Mg/Ca and Li/Mg values of the Japanese coral reference material JCp-1 for untreated and chemically-treated sub-samples. Li/Ca and Mg/Ca show comparable % decrease in concentration between the different cleaning steps, which results in similar Li/Mg values between the different cleaning steps.

Table 3. Laser ablation and solution ICP-MS Element/Ca ratios of tropical, temperate and cold-water corals. Values for the fibers correspond to FA_{eq} (selected portion of fibrous aragonite close to the expected oxygen isotopic equilibrium with ambient seawater).

Table 4. Correlations between Li/Ca, Mg/Ca and Li/Mg ratios for different coral microstructures with temperature, salinity, ΔCO_3^{2-} and $\Omega_{aragonite}$. CWC: cold-water corals; SWC: shallow-water corals; TOTAL: values corresponding to the entire laser ablation transect.

Table 5. Partition coefficients between the aragonite and the calcifying fluid for Li/Ca, Mg/Ca and Li/Mg used to model the Rayleigh fractionation. Values of $K_d^{Mg/Ca}$ were calculated using equation 7 for each sample. Values of $K_d^{Li/Ca}$ were obtained based on measured Li/Ca and Mg/Ca ratios for each sample (Table 2), the temperature-dependent $K_d^{Mg/Ca}$, Mg/Ca_{sw} and Li/Ca_{sw}. $K_d^{Li/Mg} = K_d^{Li/Ca} / K_d^{Mg/Ca}$.

REFERENCES

Adkins J. F., Boyle E. A., Curry W. B. and Lutringer A. (2003) Stable isotopes in deep-sea corals and a new mechanism for "vital effects". *Geochimica et Cosmochimica Acta* **67**, 1129 –1143.

Adkins J. F., Cheng H., Boyle E., Druffel E. and Edwards R. (1998) Deep-Sea coral evidence for rapid change in ventilation of the deep north atlantic 15,400 years Ago. *Science* **280**, 725–8.

Albarède F. (1995) Introduction to Geochemical Modeling. Cambridge University Press, 543 p.

Alibert C. and McCulloch M. T. (1997) Strontium/calcium ratios in modern *Porites* corals from the Great Barrier Reef as a proxy for sea surface temperature: Calibration of the thermometer and monitoring of ENSO. *Paleoceanography* **12**, 345–363.

Allison N. and Finch A. A. (2007) High temporal resolution Mg/Ca and Ba/Ca records in modern *Porites lobata* corals. *Geochemistry Geophysics Geosystems* **8,** Q05001.

Beck J. W., Edwards R. L., Ito E., Taylor F. W., Recy J., Rougerie F., Joannot P. and Henin C. (1992) Sea-surface temperature from coral skeletal strontium/calcium ratios. *Science* **257**, 644–647.

Bevington, P.R., Robinson, D.K., 1992. Data reduction and error analysis for the physical sciences. 2nd edition McGraw-Hill, New York, 328 p.

Brahmi C., Kopp C., Domart-Coulon I., Stolarski J. and Meibom A. (2012) Skeletal growth dynamics linked to trace-element composition in the scleractinian coral *Pocillopora damicornis*. *Geochimica et Cosmochimica Acta* **99**, 146–158.

Broecker W. S. and Peng T. H. (1982) Tracers in the sea. Eldigio Press, Palisades, New York, Lamont-Doherty Geological Observatory Columbia University, 690 p.

Cairns S. and Keller N. B. (1993) Azooxanthellate Scleractinia (Cnidaria, Anthozoa) from the tropical South-West Indian Ocean, with comments on their zoogeography and ecology. *Annals of the South African Museum* **103**, 213–292.

Cairns S. and Stanley G. (1982) Ahermatypic coral banks: living and fossil counterparts, in: Gomez, E.D., Birkeland, C.E., Buddemeier, R.V., Johannes, R.E., Marsh, J.A., and Tsuda, R.T. (Eds.), Proceedings of the 4th International Coral Reef Symposium. Manila, pp. 611–618.

Case D. H., Robinson L. F., Auro M. E. and Gagnon A. C. (2010) Environmental and biological controls on Mg and Li in deep-sea scleractinian corals. *Earth and Planetary Science Letters* **300**, 215–225.

Chisholm J. R. M. and Gattuso J.-P. (1991) Validation of the alkalinity anomaly technique for investigating calcification and photosynthesis in coral reef communities. *Limnology and Oceanography* **36**, 1232–1239.

Cohen A. L. and McConnaughey T. (2003) Geochemical Perspectives on Coral Mineralization. *Reviews in Mineralogy and Geochemistry* **54**, 151–187.

Cohen A. L., Gaetani G. A., Lundälv T., Corliss B. H. and George R. Y. (2006) Compositional variability in a cold-water scleractinian, *Lophelia pertusa*: New insights into "vital effects". *Geochemistry Geophysics Geosystems* **7,** Q12004, doi:10.1029/2006GC001354.

Dickson A. G. and Millero F. J. (1987) A comparison of the equilibrium constants for the dissociation of carbonic acid in seawater media. *Deep Sea Research Part A. Oceanographic Research Papers* **34**, 1733–1743.

Dissard D., Douville E., Reynaud S., Juillet-Leclerc A., Montagna P., Louvat P. and McCulloch M. (2012) Light and temperature effects on δ11B and B/Ca ratios of the zooxanthellate coral *Acropora* sp.: results from culturing experiments. *Biogeosciences* **9**, 4589–4605.

Dodge P., Wyers S., Frith H., Knap A., Smith R., Cook C. and Sleeter T. (1984) Coral calcification rates by buoyant weight technique: effects of alizarin staining. *Journal of Experimental Marine Biology and Ecology* **75**, 217–232.

Elderfield H. (1996) A biomineralization model for the incorporation of trace elements into foraminiferal calcium carbonate. *Earth and Planetary Science Letters* **142**, 409–423.

Erez J. (1978) Vital effect on stable-isotope composition seen in foraminifera and coral skeletons. *Nature* **273**, 199–202.

Fallon S. J., McCulloch M. T., van Woesik R. and Sinclair D. J. (1999) Corals at their latitudinal limits: laser ablation trace element systematics in *Porites* from Shirigai Bay, Japan. *Earth and Planetary Science Letters* **172**, 221–238.

Fallon S.J., McCulloch M.T., Alibert C. (2003) Examining water temperature proxies in Porites corals from the Great Barrier Reef: a cross-shelf comparison. *Coral Reefs* **22**, 389-404.

Finch A. A. and Allison N. (2008) Mg structural state in coral aragonite and implications for the paleoenvironmental proxy. *Geophysical Research Letters* **35**, 1–5.

Frank N., Paterne M., Ayliffe L., van Weering T., Henriet J.-P. and Blamart D. (2004) Eastern North Atlantic deep-sea corals: tracing upper intermediate water Δ14C during the Holocene. *Earth and Planetary Science Letters* **219**, 297–309.

Freiwald A., Fossa J. H., Grehan A., Koslov T. and Roberts J. M. (2004) Cold-water coral reefs. UNEP-WCMC, Cambridge, UK, 86 p.

Gabitov R. I., Gaetani G. A., Watson E. B., Cohen A. L. and Ehrlich H. L. (2008) Experimental determination of growth rate effect on U6+ and Mg2+ partitioning between aragonite and fluid at elevated U6+ concentration. *Geochimica et Cosmochimica Acta* **72**, 4058–4068.

Gabitov R., Schmitt A., Rosner M., McKeegan D., Gaetani G., Cohen A., Watson E. and Harrison T. (2011) In situ δ7Li, Li/Ca, and Mg/Ca analyses of synthetic aragonites. *Geochemistry, Geophysics, Geosystems*, **12**, Q03001, doi:10.1029/2010GC003322.

Gaetani G. A. and Cohen A. L. (2006) Element partitioning during precipitation of aragonite from seawater: A framework for understanding paleoproxies. *Geochimica et Cosmochimica Acta* **70**, 4617–4634.

Gaetani G. A., Cohen A. L., Wang Z. and Crusius J. (2011) Rayleigh-based, multi-element coral thermometry: A biomineralization approach to developing climate proxies. *Geochimica et Cosmochimica Acta* **75**, 1920–1932.

Gagan M. (2000) New views of tropical paleoclimates from corals. *Quaternary Science Reviews* **19**, 45–64.

Gagnon A. C., Adkins J. F. and Erez J. (2012) Seawater transport during coral biomineralization. *Earth and Planetary Science Letters* **329-330**, 150–161.

Gagnon A. C., Adkins J. F., Fernandez D. and Robinson L. (2007) Sr/Ca and Mg/Ca vital effects correlated with skeletal architecture in a scleractinian deep-sea coral and the role of Rayleigh fractionation. *Earth and Planetary Science Letters* **261**, 280–295.

Goldschmidt V. M. (1954) Geochemistry. Clarendon Press, Oxford.

Goldstein S. J., Lea D. W., Chakraborty S., Kashgarian M. and Murrell M. T. (2001) Uranium-series and radiocarbon geochronology of deep-sea corals: implications for Southern Ocean ventilation rates and the oceanic carbon cycle. *Earth and Planetary Science Letters* **193**, 167–182.

Grossman E. L. and Ku T. (1986) Oxygen and carbon isotope fractionation in biogenic aragonite: temperature effects. *Chemical Geology: Isotope Geoscience Section* **59**, 59–74.

Guilderson T. P., Fairbanks R. G. and Rubenstone J. L. (1994) Tropical temperature variations since 20,000 years ago: modulating interhemispheric climate change. *Science* **263**, 663–665.

Hathorne E. C., Felis T., Suzuki A., Kawahata H. and Cabioch G. (2013) Lithium content of the aragonitic skeletons of massive *Porites* corals: a new tool to reconstruct tropical sea surface temperatures. *Paleoceanography* **28**, 143–152.

Holcomb M., Cohen A. L., Gabitov R. I. and Hutter J. L. (2009) Compositional and morphological features of aragonite precipitated experimentally from seawater and biogenically by corals. *Geochimica et Cosmochimica Acta* **73**, 4166–4179.

Inoue M., Suzuki A. and Nohara M. (2007) Empirical assessment of coral Sr/Ca and Mg/Ca ratios as climate proxies using colonies grown at different temperatures. *Geophysical Research Letters* **34**, 12, L12611.

Isa Y. (1986) An electron microscope study on the mineralization of the skeleton of the staghorn coral *Acropora hebes*. *Marine Biology* **93**, 91–101.

Johnston I. S. (1980) The ultrastructure of skeletogenesis in hermatypic corals. *International Review of Cytology* **67**, 171–214.

Juillet-Leclerc A., Reynaud S., Rollion-Bard C., Cuif J.-P., Dauphin Y., Blamart D., Ferrier-Pagès C. and Allemand D. (2009) Oxygen isotopic signature of the skeletal microstructures in cultured corals: identification of vital effects. *Geochimica et Cosmochimica Acta* **73**, 5320–5332.

Laborel J. (1987) Marine biogenic constructions in the Mediterranean: a review. *Scientific Reports of Port-Cros National Park* **13**, 97-126.

Le Tissier M.A.A. (1990) The ultrastructure of the skeleton and skeletogenic tissues of the temperate coral *Caryophyllia smithii*. *Journal of the Marine Biological Association of the United Kingdom* **70**, 295-310.

Lewis E. and Wallace D. W. R. (1998) Program Developed for CO_2 System Calculations. Oak Ridge, Oak Ridge National Laboratory, ORNL/CDIAC-105.

Livingston H. D. and Thompson G. (1971) Trace element concentrations in some modern corals. *Limnology and Oceanography* **16**, 786–796.

Lomitschka M. and Mangini A. (1999) Precise Th/U-dating of small and heavily coated samples of deep sea corals. *Earth and Planetary Science Letters* **170**, 391–401.

López Correa M., Montagna P., Vendrell-Simón B., McCulloch M., Taviani M. (2010) Stable isotopes (d18O and d13C), trace and minor element compositions of Recent scleractinians and Last Glacial bivalves at the Santa Maria di Leuca deep-water coral province, Ionian Sea. *Deep-Sea Research II* **57**, 471–486.

López Correa M., Montagna P., Joseph N., Rüggeberg A., Fietzke J., Flögel S., Dorschel B., Goldstein S., Wheeler A., Freiwald A. (2012) Preboreal onset of cold-water coral growth beyond the Arctic Circle revealed by coupled radiocarbon and U-series dating and neodymium isotopes. *Quaternary Science Reviews* **34**, 24–43.

Lorens R. B. and Bender M. L. (1980) The impact of solution chemistry on *Mytilus edulis* calcite and aragonite. *Geochimica et Cosmochimica Acta* **44**, 1265–1278.

Lutringer A., Blamart D., Frank N. and Labeyrie L. (2005) Paleotemperatures from deep-sea corals: scale effects, *Cold-Water Corals and Ecosystems*. Springer, Berlin Heidelberg, pp. 1081–1096.

Mangini A., Lomitschka M., Eichstädter R., Frank N., Vogler S., Bonani G., Hajdas I. and Pätzold J. (1998) Coral provides way to age deep water. *Nature* **392**, 347–348.

Marriott C. S., Henderson G. M., Crompton R., Staubwasser M. and Shaw S. (2004a) Effect of mineralogy, salinity, and temperature on Li/Ca and Li isotope composition of calcium carbonate. *Chemical Geology* **212**, 5–15.

Marriott C.S., Henderson G.M., Belshaw N.S., Tudhope A.W. (2004b) Temperature dependence of δ^{7}Li, δ^{44}Ca and Li/Ca during growth of calcium carbonate. *Earth and Planetary Science Letters* **222**, 615–624.

Marshall J. F. and McCulloch M. T. (2002) An assessment of the Sr/Ca ratio in shallow water hermatypic corals as a proxy for sea surface temperature. *Geochimica et Cosmochimica Acta* **66**, 3263–3280.

Mason E.H., Montagna P., Kubista L., Taviani M., McCulloch M., Phillips B.L. (2011) Phosphate defects and apatite inclusions in coral skeletal aragonite revealed by solid-state NMR spectroscopy. *Geochimica et Cosmochimica Acta* **75**, 7446–7457.

McCulloch M., Falter J., Trotter J. and Montagna P. (2012) Coral resilience to ocean acidification and global warming through pH up-regulation. *Nature Climate Change* 2, 623–627.

McCulloch M. T., Tudhope A. W., Esat T. M., Mortimer G. E., Chappell J., Pillans B., Chivas A. and Omura A. (1999) Coral record of equatorial sea-surface temperatures during the penultimate deglaciation at Huon Peninsula. *Science* **283**, 202–204.

McCulloch M., Taviani M., Montagna P., López Correa M., Remia A. and Mortimer G. (2010) Proliferation and demise of deep-sea corals in the Mediterranean during the Younger Dryas. *Earth and Planetary Science Letters* **298**, 143–152.

Mehrbach C., Culberson C. H., Hawley J. E. and Pytkowicz R. M. (1973) Measurement of the apparent dissociation constants of carbonic acid in seawater at atmospheric pressure. *Limnology and Oceanography* **18**, 897–907.

Meibom A., Cuif J.-P., Houlbrèque F., Mostefaoui S., Dauphin Y., Meibom K. L. and Dunbar R. B. (2008) Compositional variations at ultra-structure length scales in coral skeleton. *Geochimica et Cosmochimica Acta* **72**, 1555–1569.

Meibom A., Yurimoto H., Cuif J.-P., Domart-Coulon I., Houlbrèque F., Constantz B., Dauphin Y., Tambutté E., Tambutté S., Allemand D., Wooden J. and Dunbar R. B. (2006) Vital effects in coral skeletal composition display strict three-dimensional control. *Geophysical Research Letters* **33**, 2–5.

Mienis F., de Stigter H. C., White M., Duineveld G., de Haas H. and van Weering T. C. E. (2007) Hydrodynamic controls on cold-water coral growth and carbonate-mound development at the SW and SE Rockall Trough Margin, NE Atlantic Ocean. *Deep Sea Research Part I: Oceanographic Research Papers* **54**, 1655–1674.

Mitsuguchi T. and Kawakami T. (2012) Potassium and other minor elements in *Porites* corals: implications for skeletal geochemistry and paleoenvironmental reconstruction. *Coral Reefs* **31**, 671–681.

Mitsuguchi T., Matsumoto E., Abe O., Uchida T. and Isdale P. J. (1996) Mg/Ca Thermometry in Coral Skeletons. *Science* **274**, 962–963.

Montagna P., López Correa M., Rüggeberg A., McCulloch M. T., Rodolfo-Metalpa R., Ferrier-Pagès C., Freiwald A., Goldstein S. L., Henderson G. M., Mazzoli C., Russo S., Silenzi S., Taviani M. and Trotter J. (2009) Li/Mg ratios in shallow and deep-sea coral exoskeleton as a new temperature proxy. *AGU Fall Meeting, 14-18 December, 2009, San Francisco, USA*.

Montagna P., McCulloch M. T. and Mazzoli C. (2007) The non-tropical coral *Cladocora caespitosa* as the new climate archive for the Mediterranean: high-resolution ((weekly) trace element systematics. *Quaternary Science Reviews* **26**, 441–462.

Montagna P., McCulloch M., Taviani M., Mazzoli C., Vendrell B. (2006) Phosphorus in cold-water corals as a proxy for seawater nutrient chemistry. *Science* **312**, 1788–1791.

Montagna P., McCulloch M., Taviani M., Remia A. and Rouse G. (2005) High-resolution trace and minor element compositions in deep-water scleractinian corals (*Desmophyllum dianthus*) from the Mediterranean Sea and the Great Australian Bight, in: Freiwald, A., and Roberts, J.M. (Eds.), Cold-Water Corals and Ecosystems. Springer, Berlin Heidelberg, pp. 1109–1126.

Morri C., Peirano A., Bianchi C. N. and Sassarini M. (1994) Present-day bioconctructions of the hard coral, *Cladocora caespitosa* (L.) (Anthozoa, Scleractinia), in the Eastern Ligurian Sea (NW Mediterranean). *Biologia Marina Mediterranea* **1**, 371–372.

Mucci A. (1983) The solubility of calcite and aragonite in seawater at various salinities, temperatures, and one atmosphere total pressure. *American Journal of Science* **283**, 780–799.

Okai T., Suzuki A., Kawahata H., Terashima S., Imai N. 2002 Preparation of a new Geological Survey of Japan geochemical reference material: coral JCp-1, *Geostandards Newsletter* 2**6**, 95–99.

Peirano A., Abbate M., Cerrati G., Difesca V., Peroni C., Rodolfo-Metalpa R. (2005). Monthly variations in calyx growth, polyp tissue, and density banding of the Mediterranean scleractinian *Cladocora caespitosa* (L.). *Coral Reefs* **24**, 404–409.

Raddatz J., Liebetrau V., Rüggeberg A., Hathorne E., Krabbenhöft A., Eisenhauer A., Böhm F., Vollstaedt H., Fietzke J., López Correa M., Freiwald A., Dullo W.-Chr. (2013) Stable Sr-isotope, Sr/Ca, Mg/Ca, Li/Ca and Mg/Li ratios in the scleractinian cold-water coral *Lophelia pertusa*. *Chemical Geology* **352**, 143–152.

Rayner N. A., Brohan P., Parker D. E., Folland C. K., Kennedy J. J., Vanicek M., Ansell T. J. and Tett S. F. B. (2006) Improved Analyses of Changes and Uncertainties in Sea Surface Temperature Measured In Situ since the Mid-Nineteenth Century: The HadSST2 Dataset. *Journal of Climate* **19**, 446–469.

Reynaud S., Ferrier-Pagès C., Meibom A., Mostefaoui S., Mortlock R., Fairbanks R. and Allemand D. (2007) Light and temperature effects on Sr/Ca and Mg/Ca ratios in the scleractinian coral *Acropora* sp. *Geochimica et Cosmochimica Acta* **71**, 354–362.

Reynaud-Vaganay S., Gattuso J.-P., Cuif J.-P., Jaubert J. and Juillet-Leclerc A. (1999) A novel culture technique for scleractinian corals: application to investigate changes in skeletal d18O as a function of temperature. *Marine Ecology Progress Series* **180**, 121–130.

Robinson L. F., Adkins J. F., Keigwin L. D., Southon J., Fernandez D. P., Wang S.-L. and Scheirer D. S. (2005) Radiocarbon variability in the western North Atlantic during the last deglaciation. *Science* **310**, 1469–1473.

Robinson L, F., Adkins J. F., Frank N., Alexander C., Prouty N., Roark E. B., van de Flierdt T. (in press) The geochemistry of deep-sea coral skeletons: A review of vital effects and applications for palaeoceanography. *Deep Sea Research Part II: Topical Studies in Oceanography*.

Rodolfo-Metalpa R., Richard C., Allemand D., Bianchi C. N., Morri C. and Ferrier-Pagès C. (2006) Response of zooxanthellae in symbiosis with the Mediterranean corals *Cladocora caespitosa* and *Oculina patagonica* to elevated temperatures. *Marine Biology* **150**, 45–55.

Rogers A. D. (1999) The biology of *Lophelia pertusa* (Linnaeus 1758) and other deep-water reef-forming corals and impacts from human activities. *International Review of Hydrobiology* **84**, 315–406.

Rollion-Bard C., Blamart D., Cuif J.-P. and Dauphin Y. (2010) In situ measurements of oxygen isotopic composition in deep-sea coral, *Lophelia pertusa*: Re-examination of the current geochemical models of biomineralization. *Geochimica et Cosmochimica Acta* **74**, 1338–1349.

Rollion-Bard C., Vigier N., Meibom A., Blamart D., Reynaud S., Rodolfo-Metalpa R., Martin S. and Gattuso J.-P. (2009) Effect of environmental conditions and skeletal ultrastructure on the Li isotopic composition of scleractinian corals. *Earth and Planetary Science Letters* **286**, 63–70.

Rüggeberg A., Dullo W.-Chr., Dorschel B., Hebbeln D. (2007) Environmental changes and growth history of a cold-water carbonate mound (Propeller Mound, Porcupine Seabight). *International Journal of Earth Sciences* **96**, 57–72.

Runyon R. P., Haber A., Pittenger D. J. and Coleman K. A. (1996) Fundamentals of behavioral statistics, McGraw-Hill ed. New York.

Saenger C., Affek H. P., Felis T., Thiagarajan N., Lough J. M. and Holcomb M. (2012) Carbonate clumped isotope variability in shallow water corals: Temperature dependence and growth-related vital effects. *Geochimica et Cosmochimica Acta* **99**, 224–242.

Schröder-Ritzrau A., Mangini A. and Lomitschka M. (2003) Deep-sea corals evidence periodic reduced ventilation in the North Atlantic during the LGM/Holocene transition. *Earth and Planetary Science Letters* **216**, 399–410.

Shannon R. D. (1976) Revised effective ionic radii and systematic studies of interatomic distances in halides and chalcogenides. *Acta Crystallographica Section A: Crystal Physics, Diffraction, Theoretical and General Crystallography* **32**, 751–767.

Shen G. T. and Dunbar R. B. (1995) Environmental controls on uranium in reef corals. *Geochimica et Cosmochimica Acta* **59**, 2009–2024.

Shirai K., Kusakabe M., Nakai S., Ishii T., Watanabe T., Hiyagon H. and Sano Y. (2005) Deep-sea coral geochemistry: Implication for the vital effect. *Chemical Geology* **224**, 212–222.

Sinclair D. J. (2005) Correlated trace element "vital effects" in tropical corals : A new geochemical tool for probing biomineralization. *Geochimica et Cosmochimica Acta* **69**, 3265–3284.

Sinclair D. J., Kinsley L. P. J. and McCulloch M. T. (1998) High resolution analysis of trace elements in corals by laser ablation ICP-MS. *Geochimica et Cosmochimica Acta* **62**, 1889–1901.

Sinclair D. J., Williams B. and Risk M. (2006) A biological origin for climate signals in corals—Trace element "vital effects" are ubiquitous in scleractinian coral skeletons. *Geophysical Research Letters* **33,** L17707.

Smith J. E., Risk M. J., Schwarcz H. P. and McConnaughey T. A. (1997) Rapid climate change in the North Atlantic during the Younger Dryas recorded by deep-sea corals. *Nature* **386**, 818–820.

Smith J. E., Schwarcz H. P., Risk M. J., McConnaughey T. A. and Keller N. (2000) Paleotemperatures from deep-aea corals: Overcoming "vital effects". *Palaios* **15**, 25–32.

Stoffynegli P. and Mackenzie F. T. (1984) Mass balance of dissolved lithium in the oceans. *Geochimica et Cosmochimica Acta* **48**, 859–872.

Stolarski J. (2003) Three-dimensional micro- and nanostructural characteristics of the scleractinian coral skeleton : A biocalcification proxy. *Acta Palaeontologica Polonica* 4**8**, 497–530.

Stolarski J., Vertino A. (2012) First Mesozoic record of the scleractinian *Madrepora* from the Maastrichtian siliceous limestones of Poland. *Facies* **53**, 67–78.

Swart P. K. (1981) The strontium, magnesium and sodium composition of recent scleractinian coral skeletons as standards for palaeoenvironmental analysis. *Palaeogeography, Palaeoclimatology, Palaeoecology* **34**, 115–136.

Tambutté E., Allemand D., Zoccola D., Meibom A., Lotto S., Caminiti N. and Tambutté S. (2007) Observations of the tissue-skeleton interface in the scleractinian coral *Stylophora pistillata*. *Coral Reefs* **26**, 517–529.

Tambutté S., Holcomb M., Ferrier-Pagès C., Reynaud S., Tambutté É., Zoccola D. and Allemand D. (2011) Coral biomineralization: From the gene to the environment. *Journal of Experimental Marine Biology and Ecology* **408**, 58–78.

Taviani M., Freiwald A., Zibrowius H. (2005) Deep coral growth in the Mediterranean Sea: an overview. In: Freiwald, A., Roberts, J.M., (Eds) Cold-water Corals and Ecosystems. Springer Berlin Heidelberg, 137–156.

Th*iagarajan N., Adkins J. F. and E*iler J. (2011) Carbonate clumped isotope thermometry of deep-sea corals and implications for vital effects. Geochimica et Cosmochimica Acta 75, 4425–4416.

Venn A.A., Tambutté E., Ho*lcomb M., Laurent J., Allemand* D**.,** Tambutté S. (2013) Impact of seawater acidification on pH at the tissue-skeleton interface and calcification in reef corals. Proceedings of the National Academy of Sciences 110, 1634–1639.

Vertino A*., Stolarski J., Bosellini F., Taviani M. (2013*) **Me**diterranean corals through time: from Miocene to Present. In S. Goffredo, Z. Dubinsky (Eds.), The Mediterranean Sea: Its history and present challenges, Springer Scien*ce + Business Media Dordrecht, doi: 10.1007/978-94-007-67*04-1_14.

Wallace C. (1999). Staghorn Corals of the World: A Revision of the Genus Acropora, SIRO Publishing Collingwood Vic, 421 p.

Watson E. B. (2004) A c*onceptua*l model for near-surface kinetic controls on the trace-element and stable isotope composition of abiogenic calcite crystals1. Geochimica et Cosmochimica Acta 68, 1473–1488.

Zhong S. and Mucci A. (1989*) Calcite and aragonite precip*i**ta**tion from seawater solutions of various salinities: Precipitation rates and overgrowth compositions. Chemical Geology 78, 283–299.

Zibrowius H. (1980) Les scléractiniaires de *la Méditerranée* **et** de l'Atlantique nordoriental, Mémoires de l'Insititute Océeanographique de Monaco 11, 284 pp.

Zoccola D., Tambutté E., Kulhanek E., Puverel S., Scimeca J.-C., Allemand D. and Tambutté S. (2004) Molecular cloning and localization of a PMCA P-type calcium ATPase from the coral Stylophora pistillata. Biochimica et Biophysica Acta 1663, 117–26.

Sampling location/ Culturing Lab	Latitude	Longitude	Depth (m)	Sample code	Coral species	Seawater Parameters					
						Temperature (°C)	Salinity	CO_3^{2-} (µmol/kg)	$\Delta[CO_3^{2-}]$-aragonite (µmol/kg)	$\Omega_{aragonite}$	Source of seawater carbonate data
North Atlantic											
Stjernsund (Norway)	70°15.99' - N70°15.43' N	22°27.63' - 22°29.14' E	365 - 277	POS-325-433-1; POS-325-433-2	*Lophelia pertusa*	5.9 (0.05)	34.97	121	52.6	1.69	CARINA
Stjernsund (Norway)	70°15.81' N	22°27.71' E	254	JR-111	*Lophelia pertusa*	5.9 (0.05)	34.97	121	52.6	1.69	CARINA
Sula Ridge (Norway)	64°06.53' N	008°06.87' E	250-320	POS-228-216; POS-228-217	*Lophelia pertusa*	7.52 (0.12)	35.17	120	50.1	1.72	CARINA
Sula Ridge (Norway)	64°04.95' N	08°01.630' E	283-295	VH-95-163	*Lophelia pertusa*	7.52 (0.12)	35.17	120	50.1	1.72	CARINA
Darwin Mounds (UK)	59°49.00' N	007°22.00' W	950.00	DW13831#1	*Lophelia pertusa*	6.31 (1.25)	35.20	130	58.5	1.82	CARINA
OsloFjords (Norway)	59°06.22' N	010°41.09' E	105.00	ALK-232-1050 BG	*Lophelia pertusa*	8.2 (1.0)	35.20				
NW Rockall Bank	59°17.71' N	17°04.50' W	839	POS-292-525	*Lophelia pertusa*	7.28 (0.60)	35.16	107	30.1	1.39	CARINA
NW Rockall Bank	59°11.06' N	17°12.70' W	513-519	POS-292-526-1	*Lophelia pertusa*	8.23 (0.50)	35.16	107	30.1	1.73	CARINA
PelagiaMound (UK)	55°31.37' - N55°31.09' N	015°39.34' - 15°40.76' W	835-858	POS-292-544-1	*Lophelia pertusa*	7.92 (0.70)	35.23	123	46.5	1.6	CARINA
Rockall Bank (UK)	55°31' N	15°39' W	747	MD01 2454G	*Lophelia pertusa*	8.55 (0.66)	35.25	126	50.6	1.67	CARINA
PropellerMound (UK)	52°08.89' N	012°46.31' W	729	POS-265-499	*Lophelia pertusa*	9.6 (0.50)	35.50	123	47.4	1.63	GLODAP
Porcupine Seabight (UK)	51°26' N	11°46' W	888	MD01 2463G	*Lophelia pertusa*	9.05 (0.34)	35.50	121	44.1	1.68	GLODAP
Northern Porcupine Bank (UK)	53°30.91' N	14°21.16' W	696	M61-3/634	*Lophelia pertusa*	9.38 (0.50)	35.3	125	50.8	1.68	GLODAP
Galicia Bank (Spain)	42°30.00' N	011°30.00' W	775 - 880	VH-97-351	*Madrepora oculata*	11.2 (0.50)	35.87	136	60.3	1.8	CARINA
Galicia Bank (Spain)	42°46.59' N	11°46.88' W	823	VH-97-315	*Lophelia pertusa*	11.2 (0.50)	35.87	136	60.3	1.8	CARINA
Gulf of Mexico											
GulfMexico (US)	29°09.50' N	88°01.00' W	434 - 465	GoM	*Lophelia pertusa*	9.3 (0.50)	35.10				
Equatorial Atlantic											
Offshore N'Zeta (Angola)	07°17.00' S	12°03.00' E	370	N'Zeta	*Lophelia pertusa*	8.72 (0.50)	34.82	57	-14.1	0.8	GLODAP
Mediterranean Sea											
GondolaSlide (Italy)	41°43.508' N	17°02.794' E	674-710	M701-Dive111	*Lophelia pertusa*	13.55 (0.15)	38.64	202	127.2	2.7	Luchetta et al., 2010
Santa Maria di Leuca (Italy)	39°33.878' N	18°27.150' E	556-630	M70-1-721-red; M70-1-721-white	*Lophelia pertusa*	13.65 (0.15)	38.66	202	127.0	2.69	Luchetta et al., 2010
Santa Maria di Leuca (Italy)	39°35.37' N	18°22.99' E	497	COR2-111; COR2-111(bis)	*Lophelia pertusa*	13.75 (0.15)	38.66	202	127.0	2.69	Luchetta et al., 2010
Santa Maria di Leuca (Italy)	39°27.730' N	018°24.760' E	778-750	COR2-84	*Lophelia pertusa*	13.58 (0.15)	38.66	202	127.0	2.69	Luchetta et al., 2010
Urania Bank (Italy)	36°50.390' N	13°09.361' E	440-654	M70-1-677	*Lophelia pertusa*	13.65 (0.15)	38.69	217	144.2	2.88	MedCor cruise (R/V Urania)
Southern Ocean											
Balleny Islands	66°11.200' N	162°11.000' E	760	Fbal	*Flabellum impensum*	0.75 (0.15)	34.7	79	3.1	1.04	GLODAP
Equatorial Pacific											
Moorea (French Polynesia)	17°35' S	149°50.30' W		CS MOOO3A-102	*Porites* sp.	27.1 (1.10)	36.1	270	206.0	4.2 (0.05)	GLODAP
Uitoé (New Caledonia)	22°11' S	166°06' E		NC-2001-2004	*Porites* sp.	24.4 (1.90)	35.22	227	169.0	3.9 (0.3)	GLODAP
Great Barrier Reef											
Myrmidon Reef			8		*Porites* sp.	27.4 (2)	35.2				
North Pacific											
Ishigaki island				JCp-1	*Porites* sp.	26.1 (2.05)					
Culturing experiments											
Scientific Centre of Monaco				Clado-15	*Cladocora caespitosa*	15 (0.05)	38.5				
Scientific Centre of Monaco				Clado-18	*Cladocora caespitosa*	18 (0.05)	38.5				
Scientific Centre of Monaco				Clado-21	*Cladocora caespitosa*	21 (0.05)	38.5				
Scientific Centre of Monaco				Clado-23	*Cladocora caespitosa*	23 (0.05)	38.5				
Scientific Centre of Monaco				Acro-22-200	*Acropora* sp.	22 (0.10)	38.5	240	175.0	3.69	Dissard et al. (2012)
Scientific Centre of Monaco				Acro-25-200	*Acropora* sp.	25 (0.10)	38.5	237	172.6	3.68	Dissard et al. (2012)
Scientific Centre of Monaco				Acro-28-200	*Acropora* sp.	28 (0.10)	38.5	230	166.5	3.62	Dissard et al. (2012)

Sample	Element/Ca ratios in coral skeleton		
	Li/Ca (μmol/mol)	Mg/Ca (mmol/mol)	Li/Mg (mmol/mol)
JCp-1			
Untreated sample	6.01 (0.15)	4.21 (0.05)	1.43 (0.05)
HNO_3 (0.01N)	5.24 (0.07)	3.54 (0.16)	1.48 (0.05)
HNO_3 (0.05N)	4.49 (0.15)	2.97 (0.04)	1.51 (0.05)
HNO_3 (0.05N) + $NaOH/H_2O_2$	4.27 (0.15)	2.96 (0.04)	1.44 (0.05)
HNO_3 (0.05N) + $NaOH/H_2O_2$ + Ascorbic acid/EDTA	4.46 (0.15)	3.04 (0.04)	1.47 (0.05)

Sample code	Element/Ca ratios in coral skeleton								
	Temperature (°C)	Li/Ca (µmol/mol) LA-ICP-MS/Fibres	Mg/Ca (mmol/mol) LA-ICP-MS/Fibres	Li/Mg (mmol/mol) LA-ICP-MS/Fibres	Li/Ca (µmol/mol) LA-ICP-MS/COCs	Mg/Ca (mmol/mol) LA-ICP-MS/COCs	Li/Mg (mmol/mol) LA-ICP-MS/COCs	Li/Ca (µmol/mol) Solution-ICP-MS	Mg/Ca (mmol/mol) Solution-ICP-MS	Li/Mg (mmol/mol) Solution-ICP-MS
North Atlantic										
POS-325-433-1	5.9 (0.05)	15.04 (1.45)	4.03 (0.27)	3.73 (0.35)	15.99 (1.44)	4.97 (0.29)	3.22 (0.31)			
POS-325-433-2	5.9 (0.05)	14.47 (1.78)	3.83 (0.30)	3.78 (0.33)	16.55 (1.36)	4.97 (0.24)	3.34 (0.29)	14.21 (0.44)	3.49 (0.09)	4.07 (0.08)
JR-111	5.9 (0.05)							14.25 (0.25)	3.45 (0.04)	4.13 (0.12)
POS-228-216	7.52 (0.12)	12.66 (1.59)	3.70 (0.19)	3.42 (0.36)	15.69 (1.61)	5.31 (0.24)	2.96 (0.32)	12.06 (0.53)	3.21 (0.13)	3.76 (0.08)
POS-228-217	7.52 (0.12)	12.33 (1.29)	3.38 (0.18)	3.65 (0.38)	13.11 (1.45)	3.61 (0.24)	3.64 (0.33)			
VH-95-163	7.52 (0.12)							13.80 (0.24)	3.75 (0.05)	3.68 (0.11)
DW13831#1	6.31 (1.25)	8.34 (1.23)	2.33 (0.18)	3.58 (0.48)	11.10 (1.15)	3.90 (1.12)	2.84 (0.83)	8.41 (0.27)	2.35 (0.06)	3.57 (0.10)
ALK-232-1050 BG	8.2 (1.0)	12.43 (1.03)	3.52 (0.24)	3.53 (0.31)	14.10 (1.14)	3.99 (0.19)	3.54 (0.28)	11.66 (0.33)	3.28 (0.11)	3.55 (0.09)
POS-292-525	7.28 (0.60)							10.63 (0.18)	2.95 (0.04)	3.61 (0.11)
POS-292-526-1	8.23 (0.50)							10.98 (0.19)	3.15 (0.04)	3.49 (0.10)
POS-292-544-1	7.92 (0.70)	8.26 (0.85)	2.31 (0.13)	3.58 (0.36)	11.23 (1.28)	3.06 (0.16)	3.67 (0.36)	8.28 (0.26)	2.33 (0.09)	3.55 (0.11)
MD01 2454G	8.55 (0.66)							9.82 (0.17)	2.74 (0.04)	3.59 (0.11)
POS-265-499	9.6 (0.50)	8.41 (1.24)	2.41 (0.21)	3.49 (0.47)	13.45 (1.62)	3.63 (0.19)	3.71 (0.45)	8.38 (0.16)	2.47 (0.05)	3.39 (0.07)
MD01 2463G	9.05 (0.34)							8.56 (0.15)	2.40 (0.03)	3.57 (0.11)
M61-3/634	9.38 (0.50)							10.29 (0.31)	3.09 (0.10)	3.32 (0.07)
VH-97-351	11.2 (0.50)	10.21 (1.25)	3.24 (0.18)	3.15 (0.36)	12.41 (1.64)	4.09 (0.25)	3.03 (0.38)			
VH-97-315	11.2 (0.50)							9.34 (0.16)	3.06 (0.04)	3.05 (0.09)
Gulf of Mexico										
GoM	9.3 (0.50)	9.05 (1.33)	2.71 (0.18)	3.34 (0.45)	11.39 (1.45)	3.34 (0.16)	3.40 (0.38)	8.39 (0.32)	2.54 (0.08)	3.30 (0.05)
Equatorial Atlantic										
N'Zeta	8.72 (0.50)	9.32 (0.97)	2.87 (0.17)	3.25 (0.31)	13.55 (1.20)	3.75 (0.23)	3.62 (0.33)			
Mediterranean Sea										
M701-Dive111	13.55 (0.15)	7.80 (0.87)	2.80 (0.14)	2.79 (0.30)	11.34 (1.33)	4.09 (0.28)	2.77 (0.26)			
M70-1-721-red	13.65 (0.15)	8.17 (1.00)	2.65 (0.21)	3.08 (0.40)	9.94 (1.55)	3.51 (0.23)	2.83 (0.40)			
M70-1-721-white	13.65 (0.15)	7.57 (0.72)	2.55 (0.18)	2.97 (0.31)	12.38 (0.99)	4.07 (0.17)	3.04 (0.25)	7.84 (0.20)	2.79 (0.08)	2.81 (0.06)
COR2-111	13.75 (0.15)							8.75 (0.15)	3.05 (0.04)	2.87 (0.09)
COR2-111(bis)	13.75 (0.15)							8.53 (0.15)	2.97 (0.04)	2.87 (0.09)
COR2-84	13.58 (0.15)							8.85 (0.20)	3.15 (0.12)	2.81 (0.07)
M70-1-677	13.65 (0.15)	8.41 (0.92)	2.78 (0.16)	3.03 (0.31)	9.51 (2.32)	3.10 (1.09)	3.24 (0.60)			
Southern Ocean										
Fbal	0.75 (0.15)							17.03 (0.41)	3.26 (0.11)	5.22 (0.06)
Equatorial Pacific										
CS MOOO3A-102	27.1 (1.10)							5.96 (0.10)	4.31 (0.05)	1.38 (0.05)
NC-2001-2004	24.4 (1.90)							6.33 (0.10)	3.91 (0.05)	1.62 (0.05)
Great Barrier Reef										
Myrmidon Reef	27.4 (2)	4.41 (0.31) (FA & COCs)	2.94 (0.42) (FA & COCs)	1.52 (0.18) (FA & COCs)						
North Pacific										
JCp-1	26.1 (2.05)							6.01 (0.15)	4.21 (0.05)	1.43 (0.05)
Culturing experiments										
Clado-15	15 (0.05)	11.00 (0.81)	4.16 (0.24)	2.65 (0.18)	13.79 (0.77)	6.04 (0.38)	2.28 (0.14)	10.69 (0.26)	4.22 (0.09)	2.53 (0.06)
Clado-18	18 (0.05)	9.10 (1.16)	4.20 (0.24)	2.17 (0.23)	9.41 (1.26)	4.40 (0.34)	2.14 (0.18)	9.61 (0.20)	4.25 (0.08)	2.26 (0.05)
Clado-21	21 (0.05)	7.88 (0.61)	4.16 (0.30)	1.89 (0.17)	7.73 (0.70)	3.93 (0.30)	1.97 (0.15)	7.74 (0.23)	3.70 (0.10)	2.09 (0.06)
Clado-23	23 (0.05)	7.36 (0.64)	4.10 (0.18)	1.79 (0.16)	8.34 (0.80)	4.46 (0.32)	1.87 (0.16)	7.16 (0.24)	3.88 (0.10)	1.85 (0.08)
Acro-22-200	22 (0.10)							8.85 (0.26)	4.52 (0.04)	1.96 (0.04)
Acro-25-200	25 (0.10)							7.69 (0.19)	4.52 (0.05)	1.70 (0.02)
Acro-28-200	28 (0.10)							6.97 (0.40)	4.92 (0.17)	1.42 (0.03)

	Temperature	Salinity	ΔCO_3^{2-}	$\Omega_{aragonite}$
Temperature		Linear (+); r^2 = 0.48 (N = 25)	Linear (+); r^2 = 0.84 (N = 20)	Linear (+); r^2 = 0.89 (N = 20)
Salinity			Linear (+); r^2 = 0.55 (N = 20)	Linear (+); r^2 = 0.47 (N = 20)
ΔCO_3^{2-}				Linear (+); r^2 = 0.98 (N = 20)
Li/Ca (FAeq CWC, LA-ICP-MS)	Exponential; r^2 = 0.49 (N = 15)	Linear (-); r^2 = 0.36 (N = 15)	Linear (-); r^2 = 0.17 (N = 13)	Linear (-); r^2 = 0.19 (N = 13)
Mg/Ca (FAeq CWC, LA-ICP-MS)	Exponential; r^2 = 0.18 (N = 15)	Linear (+); r^2 = 0.11 (N = 15)	Linear; r^2 = 0.06 (N = 13)	Linear; r^2 = 0.06 (N = 13)
Li/Mg (FAeq CWC, LA-ICP-MS)	Exponential; r^2 = 0.87 (N = 15)	Linear (-); r^2 = 0.71 (N = 15)	Linear (-); r^2 = 0.42 (N = 13)	Linear (-); r^2 = 0.43 (N = 13)
Li/Ca (COCs CWC, LA-ICP-MS)	Exponential; r^2 = 0.46 (N = 15)	Linear (-); r^2 = 0.40 (N = 15)	Linear (-); r^2 = 0.33 (N = 13)	Linear (-); r^2 = 0.38 (N = 13)
Mg/Ca (COCs CWC, LA-ICP-MS)	Exponential; r^2 = 0.16 (N = 15)	Linear; r^2 = 0.06 (N = 15)	Linear ; r^2 = 0.05 (N = 13)	Linear; r^2 = 0.05 (N = 13)
Li/Mg (COCs CWC, LA-ICP-MS)	Exponential; r^2 = 0.16 (N = 15)	Linear (-); r^2 = 0.31 (N = 15)	Linear (-); r^2 = 0.34 (N = 13)	Linear (-); r^2 = 0.34 (N = 13)
Li/Ca (TOTAL CWC, LA-ICP-MS)	Exponential; r^2 = 0.38 (N = 15)	Linear (-); r^2 = 0.30 (N = 15)	Linear (-); r^2 = 0.18 (N = 13)	Linear (-); r^2 = 0.19 (N = 13)
Mg/Ca (TOTAL CWC, LA-ICP-MS)	Exponential; r^2 = 0.04 (N = 15)	Linear; r^2 = 0.02 (N = 15)	Linear ; r^2 = 0.00 (N = 13)	Linear; r^2 = 0.00 (N = 13)
Li/Mg (TOTAL CWC, LA-ICP-MS)	Exponential; r^2 = 0.78 (N = 15)	Linear (-); r^2 = 0.76 (N = 15)	Linear (-); r^2 = 0.51 (N = 13)	Linear (-); r^2 = 0.55 (N = 13)
Li/Ca (FAeq CWC + FA SWC, LA-ICP-MS + Solution)	Exponential; r^2 = 0.55 (N = 49)	Linear (-); r^2 = 0.25 (N = 48)	Linear (-); r^2 = 0.40 (N = 40)	Linear; r^2 = 0.45 (N = 40)
Mg/Ca (FAeq CWC + FA SWC, LA-ICP-MS + Solution)	Exponential; r^2 = 0.37 (N = 49)	Linear; r^2 = 0.13 (N = 48)	Linear (+); r^2 = 0.27 (N = 40)	Linear (+); r^2 = 0.23 (N = 40)
Li/Mg (FAeq CWC + FA SWC, LA-ICP-MS + Solution)	**Exponential; r^2 = 0.98 (N = 49)**	Linear (-); r^2 = 0.47 (N = 48)	Linear (-); r^2 = 0.75 (N = 40)	Linear (-); r^2 = 0.81 (N = 40)

Sample Code	Temperature (°C)	$K_d^{Li/Ca}$	$K_d^{Mg/Ca}$	$K_d^{Li/Mg}$
Fbal	0.75	5.55E-03	5.22E-04	10.63
POS-325-433-1	5.9	3.58E-03	4.71E-04	7.60
POS-325-433-2	5.9	3.63E-03	4.71E-04	7.71
POS-325-433-2	5.9	3.91E-03	4.71E-04	8.30
JR-111	5.9	3.96E-03	4.71E-04	8.41
DW13831#1	6.31	3.40E-03	4.67E-04	7.28
DW13831#1	6.31	3.39E-03	4.67E-04	7.26
POS-292-525	7.28	3.36E-03	4.58E-04	7.33
POS-228-216	7.52	3.18E-03	4.56E-04	6.98
POS-228-217	7.52	3.39E-03	4.56E-04	7.44
POS-228-216	7.52	3.49E-03	4.56E-04	7.66
VH-95-163	7.52	3.42E-03	4.56E-04	7.50
POS-292-544-1	7.92	3.29E-03	4.52E-04	7.27
POS-292-544-1	7.92	3.27E-03	4.52E-04	7.23
ALK-232-1050 BG	8.2	3.23E-03	4.50E-04	7.18
ALK-232-1050 BG	8.2	3.25E-03	4.50E-04	7.23
POS-292-526-1	8.23	3.19E-03	4.50E-04	7.10
MD01 2454G	8.55	3.26E-03	4.47E-04	7.30
N'Zeta	8.72	2.95E-03	4.45E-04	6.62
MD01 2463G	9.05	3.21E-03	4.42E-04	7.26
GoM	9.3	2.99E-03	4.40E-04	6.79
GoM	9.3	2.96E-03	4.40E-04	6.72
M61-3/634	9.38	2.98E-03	4.39E-04	6.78
POS-265-499	9.6	3.11E-03	4.37E-04	7.10
POS-265-499	9.6	3.02E-03	4.37E-04	6.90
VH-97-351	11.2	2.72E-03	4.24E-04	6.42
VH-97-315	11.2	2.63E-03	4.24E-04	6.21
M701-Dive111	13.55	2.29E-03	4.04E-04	5.67
COR2-84	13.58	2.31E-03	4.04E-04	5.71
M70-1-721-red	13.65	2.53E-03	4.03E-04	6.27
M70-1-721-white	13.65	2.44E-03	4.03E-04	6.05
M70-1-677	13.65	2.49E-03	4.03E-04	6.17
M70-1-721-white	13.65	2.31E-03	4.03E-04	5.73
COR2-111	13.75	2.35E-03	4.03E-04	5.84
COR2-111(bis)	13.75	2.35E-03	4.03E-04	5.84
Clado-15	15	2.12E-03	3.93E-04	5.39
Clado-15	15	2.02E-03	3.93E-04	5.15
Clado-18	18	1.64E-03	3.70E-04	4.42
Clado-18	18	1.70E-03	3.70E-04	4.60
Clado-21	21	1.34E-03	3.48E-04	3.85
Clado-21	21	1.48E-03	3.48E-04	4.25
Acro-22-200	22	1.36E-03	3.41E-04	3.98
Clado-23	23	1.22E-03	3.35E-04	3.64
Clado-23	23	1.26E-03	3.35E-04	3.77
NC-2001-2004	24.4	1.03E-03	3.25E-04	3.16
Acro-25-200	25	1.11E-03	3.21E-04	3.46
JCp-1	26.1	8.80E-04	3.14E-04	2.80
CS MOOO3A-102	27.1	8.27E-04	3.08E-04	2.68
Acro-28-200	28	8.75E-04	3.03E-04	2.89